TOXICOLOGICAL SCIENCES **82**, 341–358 (2004)
doi:10.1093/toxsci/kfh254
Advance Access publication August 19, 2004

Modulation of Notch Processing by γ-Secretase Inhibitors Causes Intestinal Goblet Cell Metaplasia and Induction of Genes Known to Specify Gut Secretory Lineage Differentiation

Joseph Milano,* Jenny McKay,|| Claude Dagenais,† Linda Foster-Brown,* Francois Pognan,* Reto Gadient,‡ Robert T. Jacobs,||| Anna Zacco,‡ Barry Greenberg,§ and Paul J. Ciaccio,*,[1]

*Safety Assessment US, AstraZeneca Pharmaceuticals, Wilmington, Delaware, 19850; †DMPK, AstraZeneca Pharmaceuticals, Wilmington, Delaware, 19850; ‡Neuroscience, AstraZeneca Pharmaceuticals, Wilmington, Delaware, 19850; §Target Biology, AstraZeneca Pharmaceuticals, Wilmington, Delaware, 19850; |||Chemistry, AstraZeneca Pharmaceuticals, Wilmington, Delaware, 19850; and ||Safety Assessment UK, AstraZeneca Pharmaceuticals, Alderley Park, Macclesfield, Cheshire SK10 4TG, United Kingdom

Received May 26, 2004; accepted August 11, 2004

It is anticipated that γ-secretase inhibitors (γ-Sec-I) that modulate Notch processing will alter differentiation in tissues whose architecture is governed by Notch signaling. To explore this hypothesis, Han Wistar rats were dosed for up to 5 days with 10–100 μmol/kg b.i.d. γ-Sec-I from three chemical series that inhibit Notch processing *in vitro* at various potencies (Notch IC_{50}). These included an arylsulfonamide (AS) (142 nM), a dibenzazepine (DBZ) (1.7 nM), and a benzodiazepine (BZ) (2.2 nM). The DBZ and BZ caused dose-dependent intestinal goblet cell metaplasia. In contrast, the AS produced no detectable *in vivo* toxicity, despite higher exposure to free drug. In a time course using BZ, small intestinal crypt cell and large intestinal glandular cell epithelial apoptosis was observed on days 1–5, followed by goblet cell metaplasia on days 2–5 and crypt epithelial and glandular epithelial regenerative hyperplasia on days 4–5. Gene expression profiling of duodenal samples from BZ-dosed animals revealed significant time-dependent deregulation of mRNAs for various panendocrine, hormonal, and transcription factor genes. Somatostatin, secretin, mucin, CCK, and gastrin mRNAs were elevated twofold or more by day 2, and a number of candidate 'early-predictive' genes were altered on days 1–2, remaining changed for 4–5 days; these included Delta1, NeuroD, Hes1-regulated adipsin, and the Hes-regulated transcriptional activator of gut secretory lineage differentiation, the rat homolog of Drosophila atonal, Rath1. Western blotting of fecal protein from BZ-and DBZ-dosed animals exhibited increased levels of both anti-Rath1 reactive protein and anti-adipsin reactive proteins, confirming their potential value as noninvasive biomarkers of intestinal goblet metaplasia.

Key Words: **γ-secretase; Notch receptor; Notch intracellular domain; NICD; intestinal goblet metaplasia; Rath1; Hes1; adipsin; atonal.**

INTRODUCTION

Amyloid deposits constitute a primary neuropathological hallmark within vulnerable brain regions of the Alzheimer patient (Selkoe, 2001). These deposits consist predominantly of Aβ amyloid peptide and are derived from amyloid precursor protein (APP) by a series of proteolytic events, the last of which is responsible for an intramembranous COOH-terminal cleavage mediated by a multimeric complex called γ-secretase. γ-Secretase is an aspartyl protease consisting of at least four subunits that mediates processing of other type-1 transmembrane protein substrates, including Notch receptor, ErbB4 (Lee *et al*., 2002), CD44, E- and N-cadherins (Marambaud *et al*., 2003), the p75 NGF receptor (Jung *et al*., 2003), and Notch ligands Delta-1 and Jagged-2 (LaVoie *et al*., 2003). γ-Secretase inhibitors (γ-Sec-I) have been identified that effectively reduce the cleavage of APP and therefore may provide a form of therapy for Alzheimer's disease (Dovey *et al*., 2001). However, the broad substrate specificity could lead to untoward mechanism-based side-effects. For example, signals transduced from the intracellular domain of Notch (NICD) play an essential role in the cell fate decisions, cell growth and cell differentiation. Upon ligand binding, the Notch receptor is cleaved to NICD and released from the membrane. NICD is then shuttled to the nucleus where it recruits several co-factors that initiate gene transcription, including Hairy and Enhancer of split homolog-1 (Hes1) (Baron, 2003; Sasai *et al*., 1992). Hes1 inhibits differentiation of many cell types by repressing the transcription of other factors including the bHLH transcription factor Math1 (Kageyama *et al*., 2000). When the Notch signal is interrupted Hes1 is not transcribed, and Math1 transcription and functional consequences proceed unabated.

Recently Searfoss *et al*. (2003) reported that a potent Notch modulating γ-Sec-I caused intestinal goblet cell metaplasia *in vivo* in Fisher 344 rats and induced a putative Hes-1 regulated factor called *adipsin*, which may serve as a toxicity biomarker

[1] To whom correspondence should be addressed at Molecular & Investigative Toxicology, Safety Assessment US, CRDL 138, 1800 Concord Pike, AstraZeneca Pharmaceuticals, Wilmington, DE 19850. Fax: (302) 886-2341. E-mail: paul.ciaccio@astrazeneca.com.

 © Society of Toxicology 2004; all rights reserved.

for the lesion. Similar lesions caused by a potent Notch modulator, but not by a weaker Notch modulator, were observed in mice (Wong *et al*., 2004). We confirm and extend these findings by demonstrating that the goblet cell metaplasia first observed in intestinal crypts of Han Wistar rats is preceded by the mRNA induction of the Hes-1 regulated Rath1. It is also accompanied by increased levels of intestinal mucus and an mRNA expression profile representing secretory lineage differentiation, and is followed by crypt epithelial regenerative hyperplasia. While other putative substrates for γ-secretase are described in the literature, only a subset of them have been demonstrated to be true substrates in nonrecombinant systems. Furthermore, the early and sustained upregulation of Rath1 is suggestive of a causative link between Notch modulation and the metaplasia. Moreover, the absence of such toxicity in animals dosed with a weak Notch modulating γ-Sec-I suggests that it may be possible to inactivate the processing of γ-secretase substrates selectively and thereby avoid such pharmacology related toxicity.

MATERIALS AND METHODS

Reagents. The compounds (arylsulfonamide, benzodiazepine, and dibenzazepine) employed in this study were prepared by the AstraZeneca CNS Chemistry Department (Wilmington, DE) and were of >95% chemical and isomeric purity. The human T-cell lymphoma SUP-T1 (ATCC CRL-1942) was obtained from the American Type Culture Collection. Fraction V bovine serum albumin (BSA), RPMI1640 supplemented with L-glutamine and Hepes, fetal calf serum, 100 mM sodium pyruvate, penicillin/streptomycin were purchased from Mediatech (Herndon, VA). Gene reporter lysis buffer was obtained from Roche Diagnostics (Indianapolis, IN). Glutamax I, NuPage MOPS, NuPAGE MES, MES-SDS running buffer, Triacetate SDS running buffer, NuPage transfer buffer, sodium dodecyl sulfate (SDS) polyacrylamide gels, SDS loading buffer, reducing agent, and nitrocellulose or polyvinylidene difluoride (PVDF) membranes were purchased from Invitrogen (Carlsbad, CA). The rabbit polyclonal anti cleaved Notch1 (Val1744) antibody was obtained from Cell Signaling (Beverly, MA). Rabbit anti Notch1 antibody ab8925 was purchased from Novus Biologicals (Littleton, CO). Secondary antibodies conjugated to alkaline phosphatase and horseradish peroxidase for the Notch assay were purchased from Jackson ImmunoResearch (West Grove, PA), Zymed (San Francisco, CA). Sheep polyclonal anti-complement factor D (adipsin) antibody and corresponding secondary rabbit antisheep HRP for the adipsin blotting were purchased from Abcam (Austin, TX). Math1 antibody Ab and the corresponding secondary HRP antibody for Rath1 blotting were purchased from Abcam. 10× casein solution was purchased from Vector Laboratories. Enhanced chemiluminescent (ECL) (for NICD assay) or Chemi Glow West (Adipsin and Rath1) kits were obtained from Amersham (Piscataway, NJ) and Alpha Innotech Corp (San Leandro, CA), respectively.

SUP-T1 NICD assay. Human T-cell lymphoma SUP-T1 cells cultured in RPMI1640 media supplemented with 1 mM sodium pyruvate, 2 mM Glutamax I, 1× penicillin/streptomycin and 10% fetal calf serum, exposed to γ-Sec-I for 16 h. Harvested cells were washed with 200 μl of Hanks buffer once and resuspended in 13 μl lysis buffer. Cell lysates were cleared by a 5 min spin at 2800 rpm. Protein concentrations were determined using the BCA kit from Pierce (Rockford, IL). Western blotting was performed by standard approaches. Twenty μg of total protein was resolved electrophoretically on a NuPAGE 7% Tris-Acetate gel in SDS-Tris acetate buffer. Protein was transferred onto a 0.2 μm nitrocellulose membrane, blocked with 5% non-fat dry milk in Tris-Buffered Saline Tween-20 (TBS-T), and incubated overnight at 4°C with an anti-Notch rabbit polyclonal antibody (Val1744) (Cell Signaling Tech.) at a dilution of 1:1000 in the same buffer. Between washes contained TBS-T buffer. The membrane was then probed with goat-anti rabbit horesradish peroxidase (HRP) and ECL substrate. Chemiluminescence signals were then detected by exposing x-Ray films for 2–10 min. Signals were digitized on a flatbed scanner and quantified with ONE-Dscan 2.03 (Scanalytics, Inc.).

Animals and treatments. All animal treatment and anesthesia procedures were carried out in accordance with recommended guidelines set forth by the AstraZeneca (Wilmington, DE) Animal Care and Use Committee. Male *Han:Wistar substrain Crl:WI(Glx/BRL/Han)IGSBR* rats were acquired from Charles River (Cambridge, MA). All rats were approximately 7–8 weeks of age at the start of the study. Animals were fed *ad libitum* with a standard certified pelleted diet of Purina Mills International (PMI) Rodent Laboratory Chow Item # 5002. Water was provided *ad libitum*. Animals were housed individually and randomly assigned to test groups of $n = 3$. The doses of 0, 10, 30, and 100 μmol/kg selected for the three test items were based on approximate efficacy values determined from an *in vivo* APP transgenic mouse model used for screening $A\beta_{40}$ lowering in brain and plasma. The high dose of 100 μmol/kg b.i.d. was found to be sufficient to lower plasma $A\beta_{40}$ in this model for all three compounds tested (see below and Table 1). The AS was solubilized in 0.1 M Meglumine, 2% (w/v) dextrose, pH 9 (solution); the DBZ was suspended finely in 0.5% (w/v) hydroxypropyl methylcellulose (Methocel E4M) and 0.1% (w/v) Tween 80 in water, and the BZ was suspended finely in 6% (v/v) ethanol/94% (v/v) Labrafil M 1944 CS (for chemical structures, see Fig. 1). Rats were dosed for up to 5 days i.p. b.i.d. using dosing volumes of 5 ml/kg for the AS, and 2.5 ml/kg for the BZ and DBZ. Control animals received corresponding vehicles and volumes. In addition, in time-course studies, three control groups were employed and sacrificed after days 1, 3, and 5 ($n = 3$ each, totaling $n = 9$), and 5 groups each of $n = 3$ treated with the mid-dose 30 μmol/kg b.i.d. of BZ were employed and sacrificed after 1–5 days of dosing. Tissue sections were examined on each of days 1–5, after dosing, in order to define temporally the histopathological changes. At the end of the dosing regimens, animals were fasted overnight. The following morning, animals were anesthetized with carbon dioxide and euthanized by exsanguination from the abdominal aorta. Tissue sections were either snap frozen in liquid nitrogen for total RNA isolation or fixed in 10% neutral buffered formalin for histopathological assessment.

Tg2576 mutant human APP transgenic mice express a mutated form of APP ($APP_{K670N, M67L}$) associated with familial Alzheimer's disease (fAD). APP mice show elevated levels of $A\beta_{40}$ at an early age, and begin to develop Aβ deposits at about 9 months of age (Holcomb *et al*., 1999). Compounds were solubilized in 75% polyethylene glycol and 25% dH_2O (PEG 75) and administered once s.c at 100 μmol/kg to 3-month-old Tg2576 (APP) mice. Animals were sacrificed by cervical dislocation at 4 h, and plasma was isolated. Right forebrain hemispheres were removed and homogenized in 2 ml of 0.2% DEA and 50 mM NaCl. Homogenates were centrifuged at 100,000 × g, for 1 h. Recovered supernatants

TABLE 1

Brain and Plasma Ab_{40} Lowering in the Tg2576 Mutant Human Amyloid Precursor Protein (APP) Transgenic Mouse Model 4 h after Single 100 μmol/kg Doses of γ-Sec-I

γ-Sec-I drug	Brain Ab_{40} pg/mg tissue (SEM)	% Ab_{40} lowering in brain	Plasma Ab_{40} pg/μl (SEM)	% Ab lowering plasma
VC	79.19 (3.78)			
BZ	24.75 (2.93)	69	NA	NA
VC	65.74 (5.53)		4.92 (0.59)	
DBZ	19.07 (2.17)	71	1.32 (0.12)	73
VC	77.78 (1.09)		4.99 (0.87)	
AS	22.52 (3.38)	71	2.08 (0.62)	58

VC = vehicle control; BZ = benzodiazepine; DBZ = dibenzazepine; AS = arylsulfonamide.

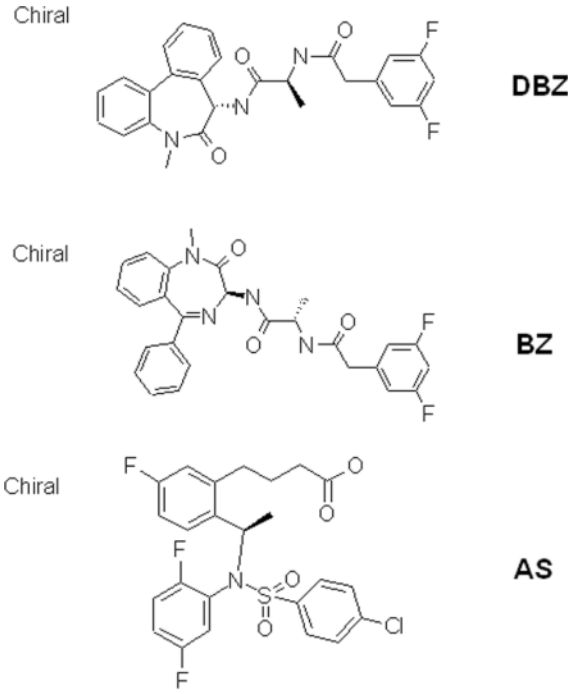

FIG. 1. Chemical structures of γ-Sec-I (dibenzazepine, DBZ; benzodiazepine, BZ; arylsulfonamide, AS).

were neutralized to pH 8.0 with 2 M Tris-HCl and diluted 1:1 in TBS, 5% fetal bovine serum (FBS), containing protease inhibitor). A Signal Select ELISA $A\beta_{40}$ kit (Biosource, Camarillo, CA) was employed to detect $hA\beta_{40}$ according to the manufacturer's instructions.

In vitro ***MDR1-MDCK cell monolayer transport experiments.*** The transport of γ-Sec I compounds across MDCK cells transfected with the human P-glycoprotein gene MDR1 was assessed in triplicate at a single time point of 60 min, at 1 and/or 10 μM, and in the presence or absence of a potent and specific inhibitor (GF120918, 2 μM; gift from Glaxo SmithKline, Research Triangle Park, North Carolina) as described elsewhere (Polli *et al*., 2001).

Determination of the plasma concentration of γ-Sec-I and pharmacokinetic analyses. Plasma was analyzed for test compounds by LC-MS-MS (MicroMass Quattro Ultima, Manchester, UK) by direct injection of supernatant following precipitation of proteins with 2 volumes of acetonitrile. Plasma protein binding was determined in duplicate at a concentration of 1 μM by equilibrium dialysis (37°C, overnight). Non-compartmental estimation of pharmacokinetic parameters was carried out with WinNonlin Enterprise 3.1 (Pharsight Corp., Mountain View, CA).

Histology and immunohistochemistry. Sections were dehydrated in graded alcohols, embedded in paraffin wax, sectioned at 5 μm, stained with hematoxylin-eosin, and examined by light microscopy. In addition, Alcian/blue periodic acid-Schiff (PAS) and Alcian blue/high iron diamine (HID) staining were carried out to ascertain the acidic versus basic and sulphomucin versus sialomucin content of goblet cells, respectively.

Cleaved caspase 3 (apoptosis marker). Sections of intestine from all control and treated animals per time point were pretreated for 10 min with 3% hydrogen peroxide. Antigen retrieval was performed using 10 min microwave pretreatment with 1 mM citrate solution. After a TBS-T wash, nonspecific protein labeling was blocked for 15 min (Protein Serum-free Block, Dako). The primary antibody (rabbit polyclonal anti-cleaved caspase-3; Cell Signaling Technology, 9661L) was diluted 1:300 and applied to sections for 60 min at room temperature. Slides were washed in TBS-T, and detection of antibody staining was then carried out using a rabbit labeled polymer method (Rabbit Envision, Dako) for 30 min and chromogenic development for 10 min with diaminobenzidine (DAB; A. Menarini). Negative controls of buffer with omitted primary and a rabbit isotype immunoglobulin (IgG) control (Dako, X0903) were used. Cleaved caspase-3 immunopositivity was scored semiquantitatively in each section by microscopically assessing the numbers of positive cells present per section. The scoring range was 0 (no positive cells) to 5 (highest numbers of positive cells).

Chromogranin A and B (pan-neuroendocrine cell marker). Sections of distal jejunum from two control and two treated animals per time point were pretreated for 10 min with 3% hydrogen peroxide. The primary antibody (rabbit polyclonal anti-Chromogranin A + B; Maine Biotechnology, PAB925NS) was diluted 1:30 and applied to sections for 60 min at room temperature. All other methodology is as described for cleaved caspase-3. Positive cells were scored semiquantitatively in the section. The score ranged from 1 (minimal positive cells) to 3 (maximal positive cells).

Total RNA isolation and gene expression profiling. To identify statistically significant changes in gene expression associated with γ-Sec-I treatment, a transcriptional profiling strategy was employed using Affymetrix high-density oligo microarrays (Santa Clara, CA). Starting material for these experiments was individual Han Wistar rat duodenum total RNA isolated from three animals per treatment group (n are listed later for each group in the captions for Figures 6 and 7, and in 4 to identify those instances where $n < 3$) Expression profiling of total RNA samples was performed using the Affymetrix rat array U34A according to the manufacturer's instructions. Briefly, total RNA was isolated using the RNeasy purification system with DNAse treatment according to the manufacturer's instructions (Qiagen, Valencia, CA). RNA concentration was determined spectrophotometrically (260/280 nm); RNA integrity was assessed by an Agilent Bioanalyzer. Samples were aliquoted to 10 μg and used as a template for double-stranded cDNA synthesis. Reverse transcription was primed using a T7-modified oligo-dT primer (5′GGCCAGTGAATTGTAATACGACTCACTATAGGG-CTCACTATAGGGAGGCGGT24-3′). *In vitro* transcription was performed on double-stranded cDNA synthesis, using a kit from Enzo Diagnostics. The resultant cRNA products were purified using RNeasy columns (Qiagen) and quantitated spectrophotometrically. For each sample, 20 μg of *in vitro* transcribed cRNA was fragmented by heating the sample to 94°C in the presence of 40 mM Tris-acetate, pH 8.1, 100 mM potassium acetate, and 30 mM magnesium acetate. Purity and quality of nucleic acids were evaluated at every step by Bioanalyzer. Hybridization cocktails contained 0.05 μg/μl of fragmented cRNA; 50 pM control B2 oligonucleotide; 1.5, 5, 25, and 100 pM of BioB, BioC, BioD, and Cre spiked cRNAs, respectively; 0.1 mg/ml herring sperm DNA; 0.5 mg/ml acetylated bovine serum albumin (BSA); 100 mM 2-(N-morpholino)ethanesulfonic acid (MES); 1 M NaCl, 20 mM ethylene diamine tetraacetic acid (EDTA); and 0.01% Tween-20. Hybridization, washing, and scanning were performed according to Affymetrix's recommendations. Image acquisition and segmentation were performed using a GeneArray Scanner (Agilent and MicroArray Suite 5.0 (Affymetrix)). Tab-delimited text file outputs containing raw fluorescence intensity data were exported for downstream analysis to Excel or GeneSpring 5.0. Gene lists were generated by comparing raw data values of each treated group to controls using one-way analysis of variance (ANOVA) $p < 0.05$ with a Benjamini-Hochberg False Discovery correction, Venn analysis, and a 1.5-fold cut-off for two of the five treatment groups in the 5-day time course.

Real-time polymerase chain reaction (PCR). Five micrograms total RNA was reverse transcribed in a 50 μl reaction using random hexamer oligonucleotides and the Superscript II reverse transcription system from Invitrogen Inc. (Carlsbad, CA) and further diluted to 25 ng/μl. Quantitative real-time PCR (QRT-PCR) was performed by creating a standard curve. Each sample was then assayed for mRNA abundance of adipsin and Rath1 using 1 μl at 25 ng/μl cDNA. Oligonucleotide primers and fluorescence resonance energy transfer (FRET) probes were obtained from Biosource International (Camarillo, CA). The 50 μl Rath1 QRT-PCRs contained 25 ng template cDNA, 200 nM each primer, 100 nM FRET probe, and 25 μl Taqman Universal Master Mix obtained from Applied Biosystems (Foster City, CA).). Adipsin QRT-PCR conditions were the same as for Rath1 except for the use of 250 nM probe in each reaction. Thermal cycling was performed on a DNA Engine Opticon 2 (manufactured by

MJ Research, Waltham, MA) using the following profile: 50°C 2 min, 94°C 10 min, then 40 cycles of 94°C 15 s, 60°C 1 min. Statistical comparisons of data were made between each treatment and the vehicle control using an unpaired *t*-test $p < 0.05$.

Adipsin

Forward 5′-GGGCAATCACCAAGAACATGAT-3′
Reverse 5′-GGAGTCGCCCCTGCAAGT-3′
Probe 5′FAM-TGTGCAGAGAGCAACCGCAGGG-TAMRA3′

Rath1

Forward 5′-AGCTGGACGCTTTGCACTTT-3′
Reverse 5′-TCTGTGCCATCATCGCTGTT-3′
Probe 5′FAM-CAGCTTTCGAGGACCGGGCCC-TAMRA3′

Rath1 and adipsin Western blotting of feces extract. Stool samples were placed in freshly prepared TBS-T containing 2× protease inhibitor cocktail sets I & III (Calbiochem, San Diego, CA) and homogenized on ice at full speed for 30 s using a Power Gen 1800G homogenizer with a 7 mm × 95 mm probe. The samples were centrifuged at 500 × g for 10 min at 4°C in a Hereaus table-top centrifuge, and the supernatant was collected. The supernatant was then centrifuged at 10, 000 × g for 5 min and again collected. Protein was determined by the method of Lowry using a kit from Pierce (Rockford, IL). Protein was resolved on 4–12% NuPage Novex Bis-Tris Polyacrylamide gradient gels (in MES buffer) and electrophoretically transferred to PVDF membranes. Membranes were blocked in TBS-T containing 1% BSA and probed with adipsin antibodies in the same buffer at 1:10, 000 dilution, and with Math1 antibodies in the same buffer at 1: 1,000 dilution. The membranes were probed with secondary rabbit anti-sheep HRP or goat anti-rabbit HRP for 1 h at room temperature. After they were washed, the blots were incubated in ChemiGlow West ECL substrate for 5 min (Alpha Innotech). Chemiluminescence signals were then detected with an Alpha Innotech Corp digital camera fitted with appropriate filters.

RESULTS

In vivo efficacy, and *in vitro* Notch inhibition. The three γ-secretase inhibitors, AS, BZ, and DBZ, were all equally effective in reducing Aβ40 levels in Tg2576 mutant APP transgenic mice (Table 2). The DBZ and AS were approximately equally effective in reducing Aβ40 plasma levels (BZ was not tested for Aβ40 plasma levels). The three γ-Sec-I exhibited differing potencies for Notch processing inhibition *in vitro* in the SupT1 model. The NICD IC_{50} for AS, DBZ, and BZ was 142 nM, 1.7 nM, and 2.2 nM, respectively (Table 3).

γ-Sec-I plasma exposure in the Han Wistar rat, and MDR1-MDCK transport. Plasma concentrations and pharmacokinetic descriptors following b.i.d. i.p. or b.i.d. oral administration on day 1 at the three dose levels established for the three γ-Sec-I are reported in Table 2. For all compounds, exposure, as

TABLE 2
***In Vitro* Notch Modulation (IC_{50}) in SupT1 Cells, and *In Vivo* Drug Exposure to γ-Sec-I in Male Han Wistar Rats ($n = 3$ unless specified otherwise) on the First Day of Dosing**

Drug	SupT1 IC_{50} (nM)	Dose (μmol/kg/day b.i.d.)	% Free rat plasma	C_{max} (SD) (nM)	Unbound C_{max} (nM)	$AUC_{(0-12h)}$ (SD) (nM h)	Unbound $AUC_{(0-12h)}$ (nM h)
BZ	2.2	10	8.5	173 (120)	14.7	1020 (670)	86.7
		30		303 (44)	25.8	2490 (400)	212
		100		284 (184)	24.1	2570 (1870)	218
DBZ	1.7	10	5.4	7.54 (3.67)	0.407	69.8 (NA)	3.77
		30		22.7 (14.4)	1.23	145 (60)	7.83
		100		81.3 (46.8)	4.39	494 (183)	26.7
AS	142	10	0.69	3520 (910)	24.3	6780 (350)	46.8
		30		14,900 (7800)	103	26,100 (7400)	180
		100		43,800 (58200)	302	117,000 (118000)	807

TABLE 3
Apparent Permeability (P_{app}) of γ-Sec-I across MDCK Cell Monolayers Transfected with Human P-Glycoprotein (MDR1-MDCK) as Determined at a Single Time Point of 60 min (average of $n = 3$)

Compound	Condition	P_{app} (AB) × 10^{-6} cm/s	P_{app} (BA) × 10^{-6} cm/s	Efflux ratio P_{app} (BA)/P_{app} (AB)	Mass balance (AB) %
DBZ	1 μM	12	64	5.3	84
	10 μM	2.9	20	6.9	79
	1 μM + inhibitor	30	36	1.2	60
BZ	1 μM	9.2	96	10	89
	10 μM	22	130	5.9	96
	1 μM + inhibitor	42	42	1.0	49
AS	10 μM	47	54	1.2	79

Note.–In some experiments, the P-glycoprotein inhibitor GF120918 was present at a concentration of 2 μM.

determined by maximum plasma concentrations (C_{max}) and area under the curve from 0 to 12 h [$AUC_{(0–12\ h)}$], was demonstrated at all doses on day 1 (Table 2). Because most of the compounds were eliminated during a dosing interval (data not shown), it was reasonable to assume that there would be no systemic accumulation after multiple doses, resulting in exposure similar to day 1. Overall, plasma exposure to DBZ after i.p. administration was the lowest of all γ-SEC-I, suggesting poor i.p. absorption and/or extensive elimination (metabolism). C_{max} and $AUC_{(0–12h)}$ appeared to increase dose-proportionally. Similarly, BZ plasma concentrations were relatively low and did not exceed 1 μM, even at the highest dose (100 μmol/kg b.i.d.), also suggesting poor absorption. Exposure appeared to increase less than dose-proportionally, but variability in the data makes this difficult to ascertain. This may have been due to slow release from the formulation and/or solubility-limited absorption, and may explain in part why the time to maximal plasma concentration (T_{max}) was relatively late (2 h in most cases and as long as 6 h in some animals, data not shown). Average AS exposure was the highest and increased slightly more than dose-proportionally (4- to 5-fold vs 3.3-fold) between 30 and 100 μmol/kg, but because variability was high, this may not be of practical significance. BZ and DBZ clearly were substrates of the efflux transporter P-glycoprotein as demonstrated by higher rates of transport in the basolateral-to-apical direction (Table 3). Inhibition of the efflux process with a specific inhibitor equalized transport in both directions, confirming substrate status. AS does not appear to be a substrate of P-glycoprotein.

Pathology. After administration of DBZ and BZ at 10, 30, or 100 μmol/kg b.i.d., there was distension of the stomach and the small and large intestines, as well as an accumulation of mucus within the intestines. The severity of these findings was dose-dependent. In the time-course study, similar intestinal changes were noted from day 1 onward after treatment with 30 μmol/kg b.i.d. There were no gross findings after AS administration, even when the dosing was extended for 30 days and despite clear *in vivo* activity of this γ-Sec-I (Table 1) at similar plasma concentrations in the APP mouse model (data not shown).

After administration of DBZ or BZ, there were significant dose-dependent compound-related histopathologic changes throughout the intestine; after DBZ administration only there was clear dose-dependent splenic marginal zone lymphoid tissue atrophy. The intestinal histopathology comprised apoptosis of small intestinal crypt epithelial cells, goblet cell metaplasia, villous stunting, villous epithelial vacuolation, and intraluminal mucus. The term *goblet cell metaplasia* is used to describe an intestinal change that comprises goblet cell hyperplasia, metaplasia (based on mucin staining property alteration), and dysplasia. There were no histopathological changes after AS administration.

Apoptosis. The earliest change observed at day 1 was apoptosis of small intestinal crypt cell epithelial cells and large intestinal glands (Fig. 2a). This was confirmed with cleaved caspase 3 immunohistochemistry (Fig. 2c). In animals given vehicle control, there was minimal cleaved caspase-3 positive staining in surface epithelial cells of villus tips and rare positive cells in small intestinal crypts (Fig. 2b). After administration of BZ, numbers of immunopositive cells increased in small intestinal crypt epithelium and colonic glands at days 1 and 2. Increased numbers of apoptotic cells occurred for the longest period—*i.e.*, 4–5 days—in duodenum and jejunum, and numbers were greater on days 1 and 2 than on subsequent days (data not shown). Increased numbers of apoptotic cells were present in the colon and ileum on days 1 and 2, respectively, but the increase was less marked than that occurring in the duodenum and jejunum.

Goblet cell metaplasia in the Han Wistar rat. Apoptosis appearing on days 1–5 was followed by goblet cell metaplasia from day 2 to day 5. This was most severe in the duodenum (Fig. 3b) and jejunum (data not shown) and increased in its distribution from day 2 (multifocal) to day 5 (diffuse). Alcian blue/PAS staining highlighted the increase in goblet cell numbers, and in AB/HID slides of distal jejunum there was a switch from sialomucin (50%) to sulphomucin (90%) production, confirming our designation of the lesion as 'metaplastic' (Fig. 3d and 3e). Small intestinal crypt epithelial cell hyperplasia and/or large intestinal glandular epithelial hyperplasia was observed at all gut levels except the cecum on days 4 and 5 of dosing (duodenum shown in Fig. 3c).

Neuroendocrine cells. In control animals, minimal numbers of chromogranin-positive cells were observed in the villi, at the base of crypts, and in the lamina propria (Fig. 4b). An increase in the number of chromogranin-positive cells was observed in treated animals from day 1 and was maximal over days 3–5 (Fig. 4a). These cells were mainly in the crypts (Fig. 4a and 4b).

Marginal zone lymphoid depletion. Lymphoid depletion in the marginal zone of the spleen was also observed from day 2, and this increased in severity as time went on (Fig. 5a and 5b). In addition, dose-dependent marginal zone lymphoid atrophy occurred after administration of DBZ and BZ. There were no histopathological changes after AS administration.

Gene expression profiling. Detailed analysis of the effects of γ-secretase inhibition on gene expression may identify novel biomarkers and help elucidate the molecular mechanisms underlying the observed gut lesion. High-density nucleic acid microarray analysis of total RNA from control and responding tissue was thus employed to identify early-predictive, global patterns of gene regulation. Microarray analysis of duodenum total RNAs revealed upregulation of several enteroendocrine factors relating to the pathologic response to γ-Sec-I that have been reported previously (Searfoss *et al.*, 2003). These relate to chronic dysregulation of elements in the Notch pathway in a pattern similar to that observed in developing embryos with Hes1 deletions (Jensen *et al.*, 2000) (Table 4). On days 1–2 in a 5-day time course, analysis of duodenum from BZ-treated animals demonstrated increased gastrin (1.0–4.1-fold), CCK

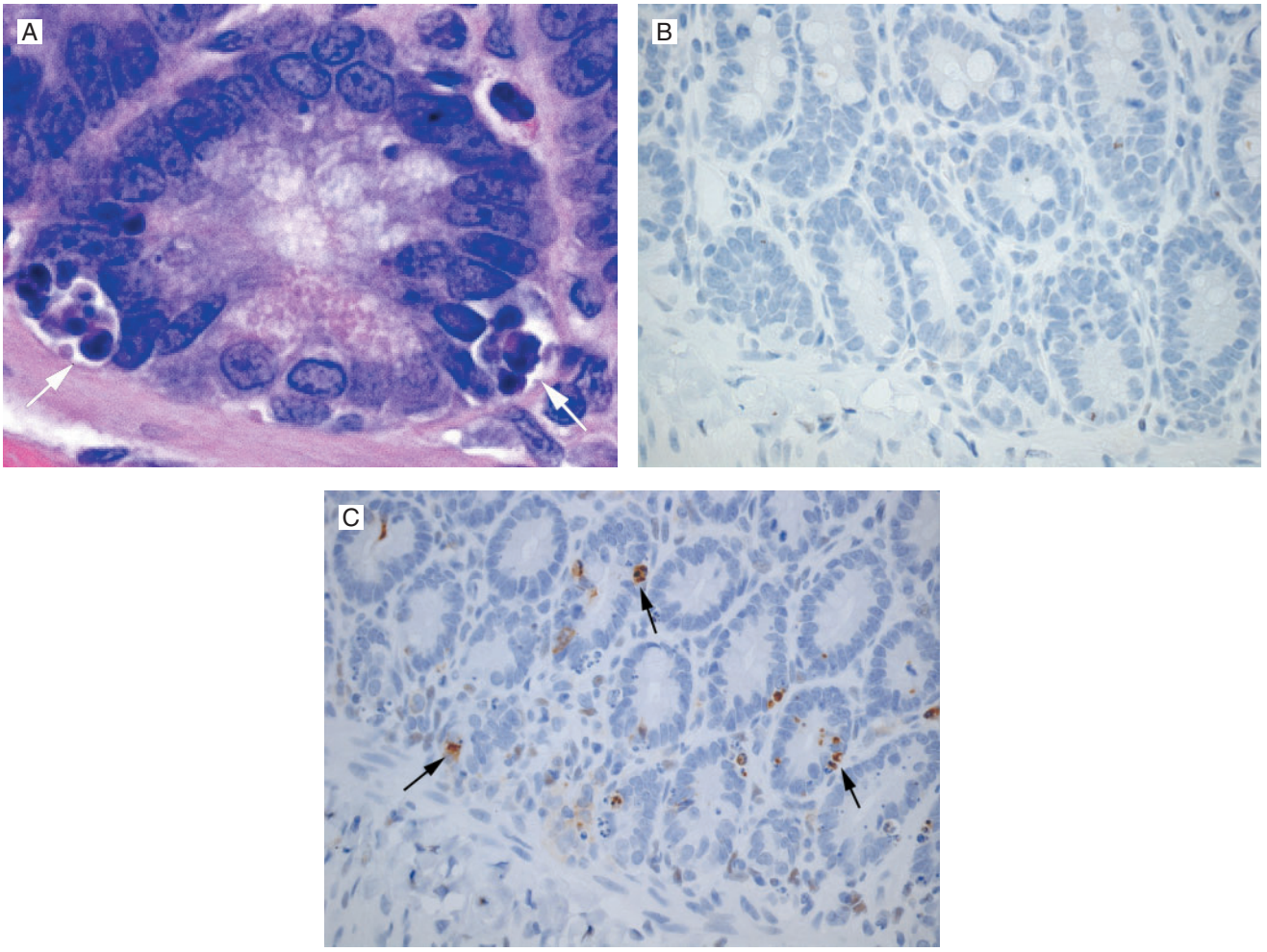

FIG. 2. γ-Sec-I that modulate Notch processing cause intestinal apoptosis. (A) Apoptosis in duodenal crypt epithelial cells (arrows) after 2 days of 30 μmol/kg b.i.d. BZ (×40 obj enlarged image, HE). (B) Cleaved caspase-3 immunopositivity is absent in the jejunal crypt epithelial cells of an animal given vehicle control and is markedly increased after 2 days administration of 30 μmol/kg b.i.d. in (C) (×40 obj, cleaved caspase 3).

(1.5–3.5-fold), secretin (1.6–5.0-fold), and somatostatin (1.0–4.0-fold) mRNAs (Table 4). Levels peaked at 4.2-fold, 5.9-fold, 9.1-fold, and 6.0-fold, respectively, that of vehicle controls by day 3, dipping slightly as crypt enterocyte regeneration commenced on days 4–5. Several elements in the Notch pathway were more abundant relative to controls on days 1 through days 4–5, including Delta1, furin, and NeuroD (Table 4). In addition, mucin, homocysteine-respondent protein, pancreatitis-associated protein, c-jun, Rab16, PPARγ, hepatocyte nuclear factor 3γ, and others were increased on days 1 through 4–5. Ontological classification of these genes revealed many involved in cell growth and maintenance, proliferation, and transport, as well as cell cycle and cell communication.

Eighty-eight genes were downregulated (Table 4). Many of these transcripts are involved in metabolism and cellular respiration. On average, the greatest magnitudes of reduction occurred by day 3. (note: whereas control samples were called 'Present,' Affymetrix signal values for several of the downregulated genes reached that of background noise and so the fold-change reduction cannot be reliably deduced.) There was an abundance of mitochondrial enzyme transcripts such as fumerase, acetoacetyl-CoA thiolase, carbamyl phosphate synthase, and succinyl-CoA synthase that decreased by day 2. Whereas increased apoptosis and caspase 3 immunoreactivity were observed in the duodenum of rats treated with BZ (Fig. 2), transcripts for caspase 3, caspase 6, and deoxyribonuclease 1 were reduced in parallel through the time course, most substantially by day 3. A rebound increase in these transcripts was not observed at the end of the 5-day time course when enterocytes in gut crypts were being regenerated.

We compared the time-course gene list shown in Table 4 to that of one generated from a 5-day end point dose–response experiment (samples collected on day 5 only) that included 10, 30, and 100 μmol/kg b.i.d. BZ and AS treatments (see *Supplementary Material*). There was considerable overlap between the gene list from the 30 μmol/kg b.i.d. BZ time course and the BZ dose–response experiment (102 probe sets of 160 on the list for the BZ time course). Despite a small number of genes

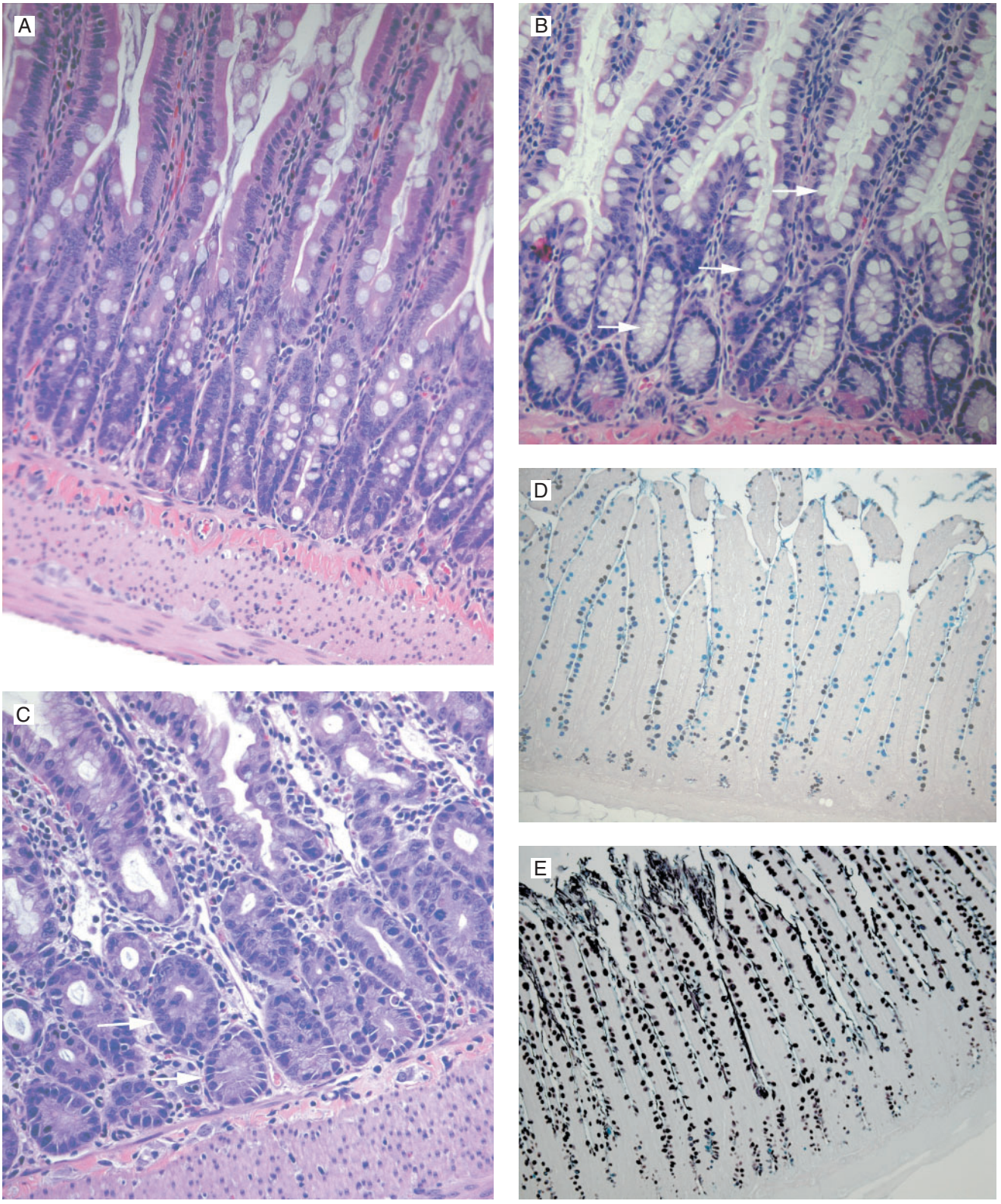

FIG. 3. γ-Sec-I that modulate Notch processing cause intestinal goblet cell metaplasia. (A) Duodenum from vehicle control (×20 obj, HE) and (B) goblet cell metaplasia (arrows) in duodenum after 3 days of 30μmol/kg b.i.d. BZ. (×20 obj, HE). (C) Crypt epithelial cell hyperplasia (arrows) in duodenum after 4 days of 30 μmol/kg b.i.d. BZ. (×20 obj, HE). (D) Jejunum from control (×10 obj, AB/HID). (E) Goblet cell metaplasia in jejunum after 5 days of 30 μmol/kg b.i.d. BZ with increased sulphomucin production (black) (×10 obj, AB/HID).

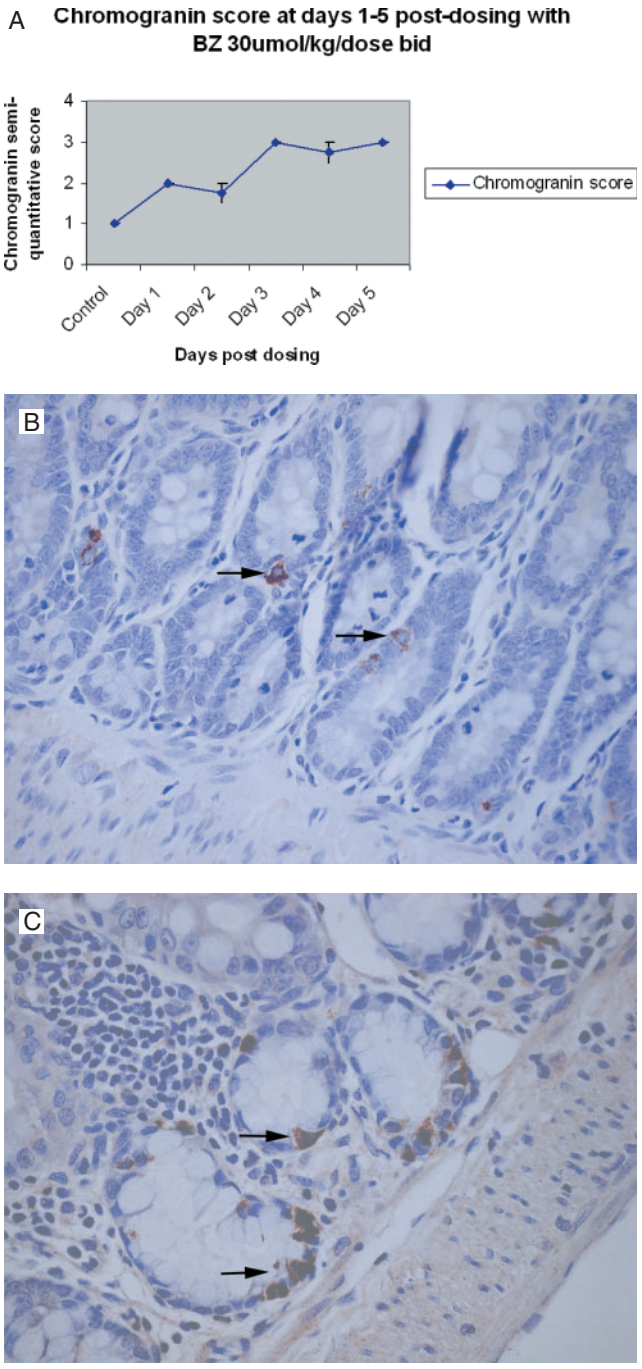

FIG. 4. Increased chromogranin staining in animals exhibiting intestinal goblet cell metaplasia. (A) Chart demonstrating the increasing number of chromogranin-positive cells in the jejunum after administration of 30 μmo/kg b.i.d. BZ. (B) Minimal chromogranin-positive cells (arrows) in jejunal crypts from a vehicle control–treated animal (×40 obj, chromogranin). (C) Increased numbers of chromogranin-positive cells in jejunal crypts (arrows) 5 days after administration of 30 μmol/kg b.i.d. BZ (×40 obj, chromogranin).

dysregulated apparently in common between one of three high-dose AS individual animal samples (also no lesion exhibited) in the 5-day dose–response experiment and that of the BZ lists, the AS changes were not statistically significant.

Rath1 and adipsin mRNA expression. *In vivo* administration in rats of a potent γ-Sec-I was recently reported to be associated with increased mRNA expression of the Hes-1 regulated gene adipsin in the gut, with a concomitant increase in the corresponding protein in fecal extracts (Searfoss *et al*., 2003). We attempted to confirm these findings in duodenum and feces matrices. In addition, because Rath1 is intimately linked to the Notch pathway, is regulated by Hes1 and we assayed the production of Rath1 and adipsin transcript in the duodenum. In an attempt to identify their earliest appearance, we also assayed Rath1 and adipsin gene products in fecal extracts and related these findings to the temporal development of the metaplastic lesion. We also sought to confirm whether expression changes of these two genes would mirror the relative Notch-modulating potency of the three test compounds, thereby strengthening the Notch culpability hypothesis. The mRNA expression of both adipsin and Rath1 was increased with BZ treatment to a maximum fold-change of 5.6 at 100 μmoles/kg b.i.d. and 4.7 at 30 μmoles/kg b.i.d., respectively. Rath1 expression fell to 2.3-fold that of vehicle control levels at the highest dose (Fig. 6A). Treatment with the most potent Notch modulator, DBZ, caused a greater increase in Rath1 mRNA than BZ. There was a 6.7-fold increase in the expression of Rath1 at the DBZ low dose and a 9.3-fold increase at the DBZ high dose (Fig. 6B). DBZ caused a 3.5-fold increase of adipsin mRNA compared to controls at the mid-dose, with more modest increases at the low and high doses. The response of Rath1 and adipsin to treatment with the AS was near control values at all doses for Rath1; it was also near control values at the low and mid-doses for adipsin, increasing to 2.6-fold at the high dose (Fig. 6C). This change was attributed to an apparent response in a single animal in the group of three.

Two independent 5-day *in vivo* time-course studies were conducted using the mid-dose 30 μmol/kg b.i.d. BZ treatment (Fig. 7A and 7B). Experiment A exhibited a temporally distinct response for Rath1 and adipsin. Rath1 mRNA increased 2.5-fold by day 1 and remained sustained throughout the time course, whereas adipsin mRNA did not increase on day 1, increased 1.5-fold by day 2, and increased 3.6-fold by day 3, falling to approximately two-fold that of control values by day 5. The mRNA expression pattern for Rath1 was similar in the two experiments. The magnitude of adipsin response was approximately similar in experiments A and B, but the time of induction differed by a day. In experiment B the increase in adipsin mRNA expression was detected on day 1 but with marked variability within the day 1 treatment group.

Western blotting of anti-Rath1 and anti-adipsin reactive fecal proteins. Whereas the molecular weight of deglycosylated rat adipsin is approximately 25 kDa, glycosylated forms resolve in the range of 38–45 kDa (Searfoss *et al*., 2003). The anti-human adipsin antibody employed in these studies recognized purified human adipsin (25 kDa) (Fig. 8, blot A, lane 1), variably recognized in fecal extracts a number of number of faint bands, including a 25 kDa protein (Fig. 8, blots A–B), and avidly

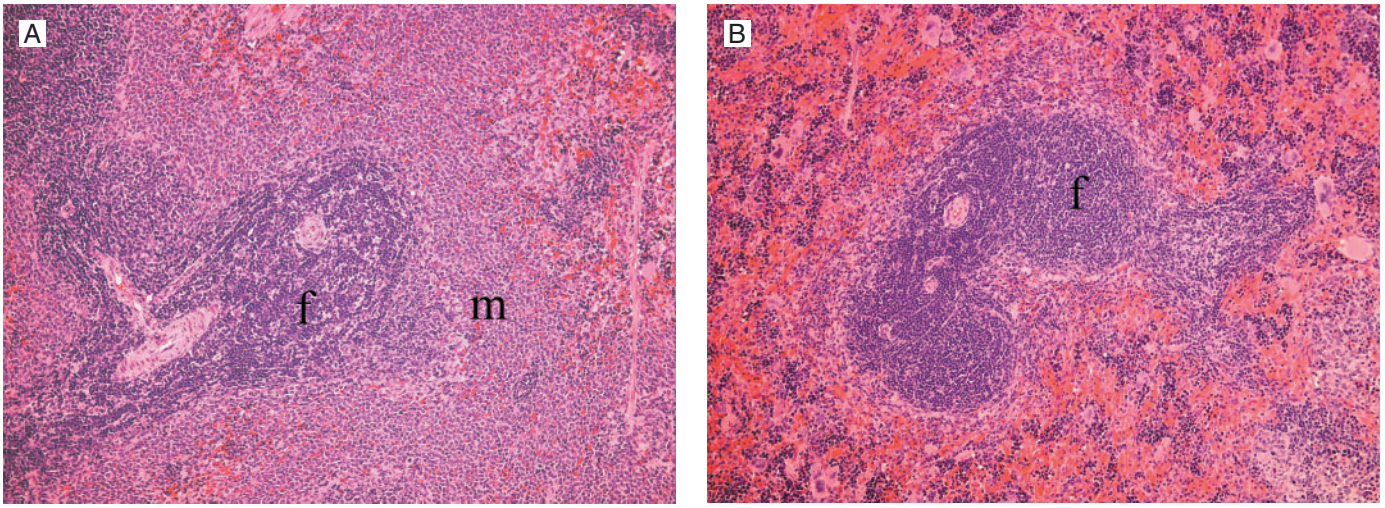

FIG. 5. Marginal zone lymphoid depletion in animals dosed with Notch-modulating γ-Sec-I. (A) Spleen from an animal after administration of vehicle control. There is a well-demarcated follicular (f) and marginal zone (m) of lymphoid cells (×10 obj, HE). (B) Spleen from an animal 3 days after administration of 30 mmol/kg b.i.d. BZ. There is loss of the marginal zone (×10 obj, HE). This lesion was observed in a dose-dependent manner in animals dosed with BZ and DBZ but not AS.

and reproducibly labeled a 6 kDa protein. This protein is likely an autolytic breakdown product or a fragment generated by residual protease in the sample. Samples maintained at 4°C for an extended period exhibit greater levels of this protein (data not shown). BZ and DBZ (blot A, lanes 4–9; blot C, lanes 2–5) but not AS (blot D, lanes 4–8) caused increased levels of this protein at doses that caused intestinal goblet cell metaplasia in a dose-dependent manner. A mid-dose of BZ (30 μmol/kg b.i.d.), which caused a moderate degree of metaplasia, increased anti-adipsin reactive protein to a level in the feces that was detectable by day 4 (blot B, days 1–3, lanes 6–8; day 4, lanes 4–5). The increased abundance of this band is sustained through day 5.

Similarly, fecal extracts were probed for Rath1 protein by western blotting (Fig. 9). The predicted molecular weight for Rath1 protein is 38 kDa. Anti-Math1 IgG detected a reactive band in extracts at 26 kDa. This size difference may also be due to residual proteolytic activity in the feces. This reactive band was detected in samples taken from animals dosed with 10 and 30 μmol/kg b.i.d. DBZ (Fig. 9A, day 5), and as early as day 3 in a 5-day time course in samples from animals dosed with 30 μmol/kg b.i.d. BZ (Fig. 9B). The anti-Math1 reactive band was present in only one of the two samples on day 3, indicating biological variability in response to the BZ. However, the increased abundance of this band was sustained through day 5.

DISCUSSION

It was anticipated that γ-Sec-I, which modulate Notch processing, will alter differentiation of specific cell populations in tissues whose architecture is governed by Notch signaling during development. Although the reported gene deletion studies of bHLH proteins in the Notch pathway demonstrate a close link between the γ-secretase complex and Notch function in the developing animal (Jensen *et al.*, 2000), the impact of γ-Sec-I treatment on the adult animal could not be predicted with certainty. To explore the effects of Notch modulation on adult tissue differentiation, 8-week-old Han Wistar rats were dosed for up to 5 days with γ-Sec-I from three chemical series that modulate Notch to varying degrees (Table 2) and that are efficacious for Aβ lowering *in vivo* (Table 1) and *in vitro* (guinea pig neuronal culture assay) (data not shown). The two potent inhibitors of Notch processing, BZ and DBZ, caused dose–dependent intestinal goblet cell metaplasia with villous stunting. In addition, there was dose–dependent atrophy of the lymphoid marginal zone of the spleen following BZ and DBZ administration. Thus, we conclude that the Notch culpability hypothesis is supported—*i.e.*, that Notch inhibition predicted the observed toxicity, because the responses mirrored the Notch-modulating potency of the three compounds, and that the failure to cause toxicity in the animals doses with AS (even following a subsequent month-long study using the same doses, data not shown) suggests that it is possible to inactivate selectively the processing of γ-Sec substrates and avoid such pronounced toxicity.

The magnitude of intestinal pathologic changes was comparable between the two potent Notch-inhibitor compounds, with DBZ being the slightly more potent of the two. However, AS did not cause these lesions, despite higher plasma free exposure than the toxic compounds (Table 2), and plasma concentrations exceeding its *in vitro* IC_{50} values for APP (data not shown) and Notch cleavage (Table 2). Although it may be considered that the free plasma concentration of AS was a smaller multiple of its *in vitro* IC_{50} than the toxic compounds, potentially causing a less complete inhibition *in vivo*, it should be noted that its unbound AUC (0–12 h)/SupT1 IC50 (=5.7) for Notch-cleavage inhibition (*i.e.*, normalized to Notch inhibitory potency) was

TABLE 4

Genes Dysregulated in Duodenum on Days 1–5 (30 μmol/kg b.i.d. BZ)

Accession number	Description	Cellular function	Raw Ctrl (n = 9)	Fold change D1 (n = 3)	D2 (n = 3)	D3 (n = 2)	D4 (n = 3)	D5 (n = 3)
Y13590	Calpastatin.	Protein kinase, protease inhibitor	7.1A	1.2	1.4	2.9	1.5	2.7
M38653	Gastrin	Enteroendocrine	10.8A	1.0	4.1	4.2	2.7	1.8
AI639109	NeuroD	Differentiation	10.9	3.1	3.8	2.5	3.8	2.2
M83679	RAB15	Intracellular traffic	10.9A	1.9	2.3	1.7	3.3	3.6
L09647	Hepatocyte nuclear factor 3a	Forkhead transcription factor	14.1A	2.2	2.4	2.3	4.3	4.0
AI070106	Serine (or cysteine) proteinase inhibitor Serpinb5	Serine proteinase inhibitor	16.6A	1.4	1.2	1.9	2.0	1.8
U17035	Mob-1	Proinflammatory cytokine	17.2	2.3	2.6	2.8	2.3	1.7
U62316	Monocarboxylate transporter 2 (MCT2) mRNA	Proton-linked monocarboxylate transporter	17.5	2.1	3.6	2.9	3.5	4.0
D15069	Adrenomedullin precursor	Hypotensive and vasodilatator	17.7A	1.4	1.7	2.0	1.3	2.1
U78889	Delta 1	Proliferation	18.0A	2.6	2.0	1.8	2.0	1.4
M92059	Adipsin	Serine protease	18.7A	1.4	2.3	3.6	1.9	2.7
M26534	Kallikrein-like serine protease (RSKG-50)	Serine protease	25.3A	1.2	1.1	2.0	1.5	1.7
M83681	RAB16	Vesicular trafficing	25.5	2.2	2.5	2.3	2.7	3.9
AA894273	EST198076	Unknown	26.9A	1.6	2.1	3.7	3.0	3.3
X70521	Amiloride sensitive Na + channel protein	Transport	27.5A	2.4	2.1	1.9	3.0	2.1
L25331	Lysyl hydroxylase mRNA	Collagen biosynthesis	29.2A	1.4	1.9	2.1	1.7	1.7
AA998338	Human phospholipase D2 splice variant hPLD2a	Transduction	31.0A	1.4	1.9	2.3	1.6	1.4
X55183	Schwannoma-derived growth factor	Mitogen	32.0	1.9	3.8	7.6	3.8	4.7
U21101	Cyclic GMP–stimulated phosphodiesterase	Outer membrane	32.4A	1.4	1.7	2.2	2.6	4.0
AB011365	PPAR-gamma protein	Peroxisomal b-oxidation of fatty acids	37.5A	2.0	2.1	1.9	1.5	0.7
D26393	Type II hexokinase	Metabolism, glycolysis	40.7	2.7	6.5	12.1	6.4	12.0
U07615	RNU07615 mucin mRNA	Epithelial coating	44.1	2.0	3.7	6.1	5.4	5.1
Z29072	Muc-2	Intestinal mucin	47.2	1.8	3.9	3.2	4.0	3.7
M91235	Rat VL30 element mRNA	Transposable element	47.6	2.1	4.6	18.1	6.6	8.1
U91679	ETS domain transcription factor PET-1	Transcriptional enhancer	49.0	1.4	2.4	1.9	1.7	1.4
AF036537	Homocysteine respondent protein HCYP2 mRNA	Apoptosis	52.2A	1.6	1.7	6.2	2.1	4.6
AF016503	Procollagen C-proteinase enhancer protein (PCPE)	Calcium -ependent receptor signaling	54.1A	1.1	1.5	2.2	1.6	1.4
S56464	Hexokinase II [rats. epididymal fat pad.]	Metabolism, glycolysis	54.4A	2.0	2.9	5.8	4.1	7.1
D30666	Brain acyl-CoA synthetase II	Fatty acid metabolism	58.5	2.0	2.4	4.5	2.7	3.5
AF036537	Homocysteine respondent protein	Apoptosis	60.8A	2.3	2.6	10.4	3.0	6.2
U87627	Putative monocarboxylate transporter	Transport	65.8A	2.5	2.2	3.4	1.5	0.9
AB017044	Hepatocyte nuclear factor 3 gamma	Forkhead transcription factor	66.8	2.4	3.1	3.4	4.2	3.9
D64050	Tyrosine phosphatase	Sequesters MAPKs in the cytoplasm	84.6	1.9	3.9	3.2	1.2	0.6
AI179610	Heme oxygenase	Transport, respiration	97.2	2.4	1.8	2.6	1.9	2.1
U60578	Carbonic anhydrase II	pH regulation	103.7	2.6	3.0	1.7	1.8	0.2
X55660	Furin	Golgi, Pro-protein cleavage	104A	1.8	2.1	2.1	1.3	0.9
X01032	Brain mRNA for cholecystokinin (CCK) precursor	Release of pancreatic enzymes in the gut	107.9A	1.5	3.5	5.9	3.2	1.4
M64030	Secretin	Enteroendocrine	110.0	1.6	5.0	9.1	6.7	1.9
AI175959	C-jun proto oncogene	Differentiation, proliferation	124.7	1.9	3.7	2.3	1.5	1.0
M60921	B-cell translocation gene 2	Anti-proliferative protein	175.2	1.8	2.8	3.9	1.7	1.4
AA955306	Ras-related protein Rab10	Signal transduction	186.6A	1.4	1.4	2.1	1.5	1.1

AI177256	EST	Similar to mouse vinculin	213.1	2.3	3.8	2.8	2.9	2.5
M25890	Somatostatin	Enteroendocrine	238.7	1.0	4.0	6.0	3.8	1.4
NM007652	CD59	Inhibitor of complement MAC	307.5	1.4	2.8	4.6	2.5	3.4
L26292	FSH-regulated protein	TGF-beta 1-stimulated	320.0	1.8	2.4	1.8	1.7	1.5
M30581	Oganellar Ca-$^{2+}$ pump mRNA.	Calcium transport	388.4	1.9	2.1	2.0	3.0	3.2
D30649	Phosphodiesterase I	Cleaves phosphodiester bonds	414.7	1.7	2.5	1.3	1.1	0.7
S81497	Lysosomal acid lipase	Intracellular hydrolysis of triglycerides	428.0	1.8	2.7	2.5	1.3	0.5
M32783	RATENKA3 dynorphin gene	Opiod neuropeptide	454.4	2.0	3.6	4.0	2.9	2.3
L20869	Pancreatitis-associated protein III (PAPIII0)	Secreted stress protein	841.2	2.9	2.1	2.2	2.2	2.3
X03478	Androsterone UDP-glucuronosyltransferase	Conjugation and elimination of toxic xenobiotics	20.5	−1.1	1.1	−6.4	−1.6	−2.4
M23995	Aldehyde dehydrogenase	Can convert/oxidize retinaldehyde to retinoic acid.	21.8	−1.8	−4.0	−27.3	−2.2	−20.4
AA859937	EST		25.9	−2.7	−1.5	−2.0	−1.2	−2.5
AA891759	EST	Hypothetical protein	28.2	−2.3	−1.9	−1.3	1.0	1.0
AA819643	AMP-activated protein kinase	Regulates cholesterol synthesis	30.8	−1.8	−1.7	−2.9	−1.3	−2.1
D63860	BMP3 Rat mRNA for prepro bone morphogenetic protein-3	Skeletal development, ossification	37.4	−3.3	−12.7	−18.2	−3.5	−14.6
AF055286	Potential-sensitive polyspecific organic cation transporter OCT3	Mediates organic cation transport	39.2	−1.9	−4.4	−3.0	−1.8	−5.1
U82591	Putative c-Myc-responsive	Rat RCL (Rcl) mRNA	39.5	−2.2	−2.4	−1.8	1.1	1.1
U77829	ESTs	Rat gas-5 growth arrest homolog non-translated mRNA	44.7	−1.7	−2.0	−1.4	−1.1	−1.1
U50412	Phosphoinositide 3-kinase p85	Necessary for the insulin-stimulated increase in glucose uptake	45.1	1.0	−2.6	−3.3	−1.1	−4.9
AA892630	EST, Weakly similar to I52331 NAD^{+} ADP-ribosyltransferase [*Rattus .norvegicus*]	Mouse poly-(ADPribosyl)-transferase homolog PARP mRNA	45.9	−1.3	−1.5	−2.4	−1.2	−2.1
S76758	Human brain-derived neurotrophic factor		52.1	−1.7	−2.0	−2.3	−1.1	−1.1
D30735	Augmenter of liver regeneration (ALR)	Liver regeneration and spermatogenesis	56.2	−1.8	−2.6	−2.4	−1.5	−1.5
AA892799	EST, weakly similar to 3-phosphoglycerate dehydrogenase [*Rattus norvegicus*]	Highly similar to human glyoxylate reductase	58.9	−1.5	−2.3	−5.7	−2.0	−2.1
X58828	Protein tyrosine phosphatase, non-receptor type 2	DNA-binding, Hydrolase	59.8	−1.8	−1.7	−1.6	−1.3	−1.3
X93591	Mismatch repair protein	DNA repair	62.1	−1.6	−1.6	−1.3	−1.1	−1.2
K03041	Ornithine carbamoyltransferase mRNA	Arginine biosynthesis	67.3	−1.6	−2.5	−5.3	−2.0	−11.7
U33500	*R.s norvegicus* retinol dehydrogenase type II mRNA, complete cds		69.6	−1.2	1.0	−13.4	−1.9	−9.0
S77492	Bone morphogenetic protein 3	Amylophosphorylase	72.2	−3.5	−6.4	−12.8	−3.8	−6.8
AA892300	EST	Intracellular protein traffic	72.9	−1.1	1.0	−1.7	−1.5	−1.9
X56917	Inositol 1,4,5-triphosphate 3-kinase	Calmodulin binding	73.0	−1.8	−3.1	−18.9	−3.6	−3.8
AA799741	EST189238 *R. norvegicus* cDNA, 3′ end	Putative ATP-dependent mitochondrial RNA helicase	74.6	−1.5	−2.4	−2.7	−1.5	−1.7
M59814	Eph receptor B2 (ELK-related protein tyrosine kinase)	Tyrosine kinase	76.0	−1.5	−2.1	−3.6	−2.0	−3.1
AA799964	EST189461 *R. norvegicus* cDNA, 3′ end		79.9	−1.1	1.1	−2.1	−1.0	−1.7
AA893717	EST		95.8	−2.4	−3.3	−1.6	1.3	1.3
S72505	Glutathione-S-transferase, alpha type (Ya)	Conjugation of reduced glutathione to hydrophobic electrophiles	100.4	−1.4	−1.3	−2.6	−1.9	−2.1
U64030	dUTPase	Nucleotide and nucleic acid metabolism	102.0	−2.9	−3.1	−2.1	1.0	1.0
M99567	Rat phospholipase C beta-3	Membrane lipid metabolism	118.2	−1.3	−2.1	−5.4	−1.9	−4.2
U76635	Deoxyribonuclease I	Apoptosis	118.8	1.0	−1.3	−12.8	−2.0	−16.1
AI171734	Rat mitochondrial fumarase mRNA	Tricarboxylic acid cycle	134.2	−1.2	−1.9	−4.8	−1.4	−1.6
U17565	Mini chromosome maintenance deficient 6 (*Saccharomyces cerevisiae*)	DNA replication	149.6	−2.7	−3.3	1.3	1.4	1.3
X62660	Glutathione transferase subunit 8	Phase II conjugation of reduced glutathione to hydrophobic electrophiles. Cytoplasmic	159.5	−1.4	−2.7	−6.3	−1.9	−3.5
S82579	Histamine N-methyltransferase	Inactivates histamine by N-methylation	162.5	−3.7	−14.2	−98.5	−6.9	−82.6

TABLE 4 *continued*

Accession number	Description	Cellular function	Raw Ctrl (n = 9)	Fold change D1 (n = 3)	D2 (n = 3)	D3 (n = 2)	D4 (n = 3)	D5 (n = 3)
L14001	RATPIGRA polymeric immunoglobulin receptor	Membrane bound Ig receptor	163.3	−1.4	−2.6	−9.3	−1.7	−3.2
AF080468	Putative glycogen storage disease type 1b protein	Carbohydrate metabolism and uptake	166.9	−1.2	−1.4	−3.2	−1.4	−2.9
M99567	Rat phospholipase C beta-3	Membrane lipid metabolism	167.0	−1.3	−2.3	−3.6	−1.7	−3.5
H31363	EST, Mouse peroxisomal membrane anchor protein (Pex14)	Involved in import of peroxisomal matrix proteins	184.7	1.1	1.0	−2.7	−1.5	−1.9
X81395	Carboxylesterase 1	Endoplasmic reticulum-targeting protein of beta-glucuronidase	191.9	−1.8	−2.8	−20.9	−5.4	−10.8
U18314	Thymopoietin (lamina associated polypeptide 2)		194.4	−1.8	−2.1	−1.8	−1.1	−1.4
AA945583	Hydroxysteroid (17-beta) dehydrogenase 10	Human amyloid beta-peptide binding protein	194.9	−1.4	−1.7	−2.3	−1.5	−1.8
D13921	Mitochondrial acetoacetyl-CoA thiolase	Role in ketone body metoabolism	204.1	−1.1	−1.2	−3.8	−1.6	−2.3
U49930	Caspase 3, apoptosis related cysteine protease (ICE-like cysteine protease)	Activation cascade of caspases responsible for apoptosis	209.8	−1.1	−1.7	−17.8	−1.1	−9.6
AF080468	Putative glycogen storage disease type 1b protein	Carbohydrate metabolism and uptake	220.5	−1.1	−1.3	−2.6	−1.3	−2.5
AA875257	EST, mouse histone H2A	Nuclear structural protein	221.9	−2.0	−2.3	−1.4	−1.1	−1.3
AA891872	EST, highly similar to NNTM NAD(P) TRANSHYDROGENASE. MITOCHONDRIAL PRECURSOR [*Mus musculus*]	Mouse mRNA for NADP transhydrogenase.	225.6	−1.7	−1.8	−2.9	−1.7	−2.4
AA899854	Topoisomerase (DNA) II alpha	Nucleic acid synthesis and modification	225.9	−2.7	−4.0	−1.6	1.1	−1.1
M85183	Angiotensin/vasopressin receptor (AII/AVP)	G protein–coupled receptor	254.6	−1.2	−2.0	−22.1	−2.0	−18.8
AA892789	EST, similar to human eukaryotic translation initiation factor 3 subunit eIF3	Protein biosynthesis	259.9	−1.7	−2.2	−3.0	−1.6	−1.7
AA874874	EST, highly similar to alcohol dehydrogenase class II	Fatty acid metabolism	266.8	−1.6	−1.9	−2.2	−1.2	−1.3
AI176621	Iron-responsive element-binding protein	RNA binding	281.7	−1.2	−1.6	−3.6	−1.7	−2.1
AF025670	Caspase 6 (Mch2)	Apoptosis	307.0	1.1	−1.8	−3.7	−1.3	−2.2
AA859688	EST, highly similar to AU RNA-binding enoyl-coenzyme A hydratase	Nuclear gene for mitochondrial product.	309.5	1.1	−1.2	−2.1	−1.4	−1.6
M11710	Nucleus-encoded mitochondrial carbamyl phosphate synthetase I gene	ATP binding	362.3	−2.1	−4.1	−13.6	−3.2	−14.0
U14647	Interleukin 1beta converting enzyme	Thiol protease that cleaves IL-1beta	377.8	−1.2	−1.9	−6.8	−1.5	−6.3
S72506	Glutathione-S-transferase, alpha type (Yc)	Phase II conjugation of reduced glutathione to hydrophobic electrophiles	443.7	−2.1	−3.8	−45.3	−3.5	−9.9
AA891914	EST, moderately similar to ACY1HUMAN AMINOACYLASE-1 [*Homo sapiens*]	Amino acid transport and metabolism	450.7	−1.1	−1.6	−2.4	−1.4	−1.7
M86235	Ketohexokinase	Carbohydrate metabolism	467.0	−1.1	−1.3	−6.5	−2.7	−5.0
AA894174	Electron transfer flavoprotein (ETF) alpha-subunit DNA. 3′ end	Electron transport	468.5	1.0	−1.3	−2.3	−1.5	−1.7
AA894174	Electron transfer flavoprotein (ETF) alpha-subunit DNA. 3′ end	Electron transport	471.3	1.0	−1.2	−2.3	−1.3	−1.6
AF095741	Hypotheitical protein MG87	Formation of diverse sulfur-metal clusters	474.8	−1.1	1.0	−3.0	−1.6	−2.7
U68562	Heat shock protein 60 (liver)	Stress response	476.0	−2.0	−3.0	−3.7	−1.2	−1.5
J03621	Mitochondrial succinyl-CoA synthetase alpha subunit (cytoplasmic precursor)	Tricarboxylic acid cycle	513.0	−1.4	−1.6	−2.1	−1.5	−1.6
S45663	Synaptic glycoprotein SC2	Highly similar to human synaptic glycoprotein	677.9	−1.1	−1.4	−2.7	−1.4	−1.7

J02592	Glutathione S-transferase Y-b subunit	Olfactory phase II conjugation of reduced glutathione to hydrophobic electrophiles	697.7	−1.2	−1.5	−4.3	−1.7	−3.5
M24542	Rieske iron-sulfur protein	Electron transport	717.6	−1.1	−1.4	−3.8	−1.4	−2.0
S87522	ESTs, highly similar to leukotriene A-4 hydrolase [*R.norvegicus*]	Leukotriene metabolism	770.0	1.0	−1.6	−4.0	−1.5	−3.0
AI170613	Heat shock 10 kD protein 1 (chaperonin 10)	Stress response	774.8	−1.8	−2.9	−2.5	−1.2	−1.4
AI170613	Heat shock 10 kD protein 1 (chaperonin 10)	Stress response	814.8	−2.1	−2.5	−1.8	−1.2	−1.3
S79676	Interleukin 1beta converting enzyme	Thiol protease that cleaves IL-1BETA	849.8	1.0	−1.9	−7.7	−1.6	−5.4
U72741	Lectin, galactose binding, soluble 9 (galectin-9)	Adhesion and molecular recognition, lectins	876.7	1.1	−1.5	−3.8	−1.3	−1.7
AI639530	EST, similar to mouse murine retrovirus readthrough RNA sequence	Mouse murine retrovirus readthrough RNA sequence	876.8	−1.4	−2.9	−14.0	−2.5	−1.9
AI179613	Mitochondrial glutamate dehydrogenase	Amino acid metabolism	1068.8	−1.3	−1.8	−3.3	−1.7	−2.3
S87522	ESTs, highly similar to leukotriene A-4 hydrolase [*R.norvegicus*]	Leukotriene metabolism	1083.8	1.0	−1.4	−3.7	−1.6	−2.4
D10952	Cytochrome c oxidase subunit Vb	Mitochondrial electron transport	1108.4	1.0	−1.2	−1.9	−1.3	−1.6
S82820	Glutathione-S-transferase, alpha type (Yc)	Phase II conjugation of reduced glutathione to hydrophobic electrophiles	1173.4	−1.8	−3.1	−12.6	−2.8	−5.8
M15327	Alcohol dehydrogenase (ADH)	Zinc dependent ADH	1258.7	−4.8	−11.2	−20.9	−7.1	−15.7
M12335	Nucleus-encoded mitochondrial carbamyl phosphate synthetase I gene, exon 13	ATP binding	1419.0	−2.1	−3.3	−33.2	−4.1	−39.3
X54793	Heat shock protein 60 (liver)	Mitochondrial matrix protein P1	1487.9	−1.8	−2.5	−2.1	−1.3	−1.4
U01145	*Rattus norvegicus* clone 15 polymeric immunoglobulin receptor mRNA, 3′UTR microsatellite repeats		1575.8	−1.4	−2.3	−7.4	−2.2	−3.2
L13025	RATPOLYIM Rat mRNA for polymeric immunoglobulin receptor	Membrane bound Ig receptor	1633.4	−1.4	−2.0	−6.6	−1.9	−2.9
J03752	Glutathione S-transferase	Mitochondrial orm	1641.9	−1.4	−2.4	−6.8	−2.3	−3.1
X53504	ESTs, highly similar to RL12 rat 60s ribosomal protein L12	Structural protein of ribosome	1922.3	−1.6	−2.1	−1.7	−1.2	1.0
L13235	RATPOLIGRA polymeric immunoglobulin receptor	Membrane bound Ig receptor	2003.1	−1.3	−1.8	−5.9	−1.7	−3.3
L14003	RATPIGRC polymeric immunoglobulin receptor	Membrane bound Ig receptor	2008.2	−1.4	−1.8	−5.6	−1.8	−2.6
L13237	RATPOLIGRB polymeric immunoglobulin receptor	Membrane bound Ig receptor	2015.7	−1.4	−1.8	−5.4	−1.8	−3.2
AI639486	ESTs, weakly similar to carboxylesterase [*H.sapiens*]		2136.9	−1.1	−1.5	−8.4	−3.2	−30.2
U32681	Deleted in malignant brain tumors 1	Rat ebnerin mRNA	2364.0	−1.7	−5.3	−26.1	−2.1	−1.8
U32681	Deleted in malignant brain tumors 1	Rat ebnerin mRNA	3401.5	−1.6	−4.9	−13.0	−2.0	−1.8

Note.–Messenger RNAs expressed in control samples that were identified as 'Absent' by Affymetrix MAS 5.0 are listed with an 'A' in the signal column. All control sample mRNAs in the group of downregulated genes and all treatment sample mRNAs in the group of upregulated genes shown were termed 'Present.'

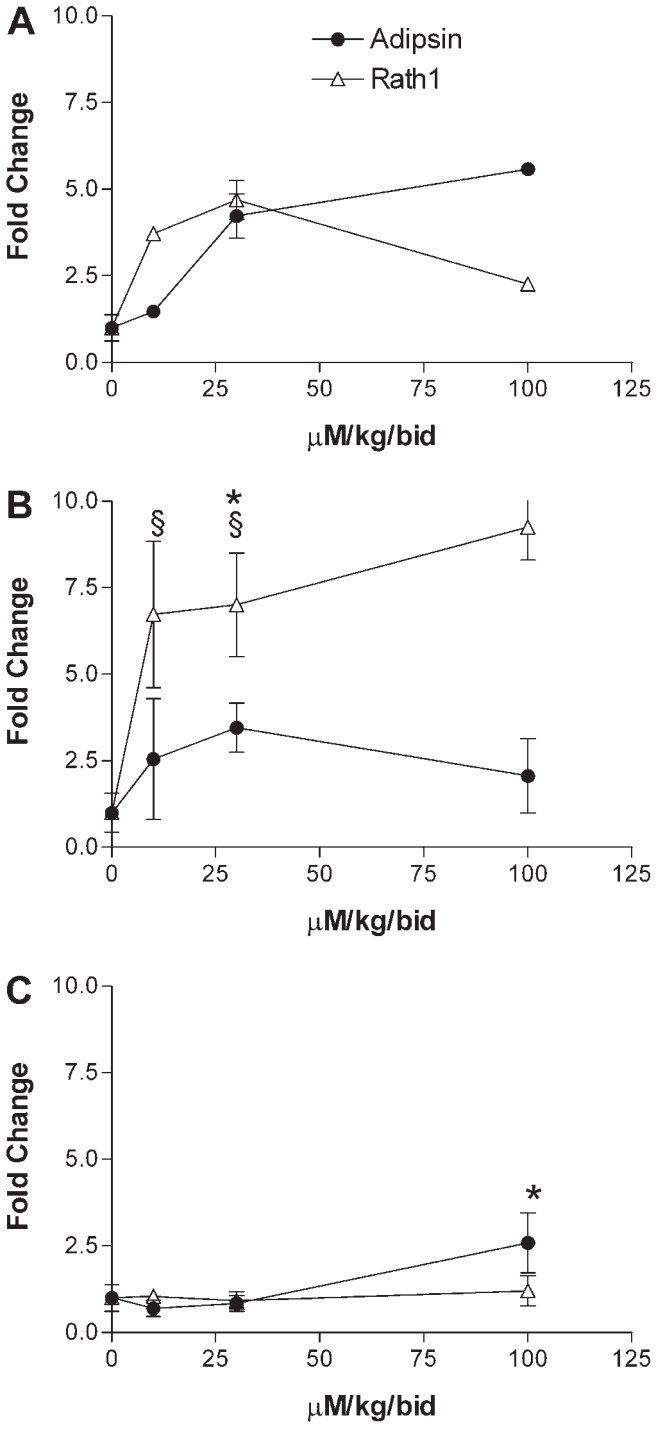

FIG. 6. Real-time polymerase chain reaction analysis of Rath1 and adipsin transcripts in duodenum total RNA. Hes1 is a transcription repressor under the control of Notch; Rath1 is a bHLH transcription factor under Hes1 control; adipsin is under Hes1 control. (A) Samples taken from animals dosed with 10 ($n = 2$), 30 ($n = 2$), and 100 ($n = 1$) μmol/kg b.i.d. BZ. (B) Samples taken from animals dosed with 10 ($n = 3$), 30 ($n = 3$), and 100 ($n = 2$) μmol/kg b.i.d. DBZ. (C) Samples taken from animals dosed with 10 ($n = 3$), 30 ($n = 3$), and 100 ($n = 2$) μmol/kg b.i.d. AS.. The symbols § and * indicate $p < 0.05$ for Rath1 and adipsin, respectively, in an unpaired *t*-test that compared treatments vs controls where $n = 3$.

similar to the same ratios for the most toxic compound, DBZ, at the two lowest doses (unbound AUC/SupT1 IC_{50} = 2.2 and 4.6). Therefore, three options are still possible: (1) that the differences between SupT1 and gut progenitor cell milieu are different enough to yield a differing dose–response curve for Notch-processing inhibition (*e.g.*, gut being less sensitive), (2) that the concentration reaching the target cells differed from what the free plasma concentration indicates, or (3) the lesion is caused in part by altered processing of other γ-secretase substrates that are also expressed in the gut (*e.g.*, ERBb4).

Both BZ and DBZ were shown to be substrates of the efflux transporter P-glycoprotein in MDR1-MDCK cells, which is expressed apically in enterocytes and endothelial cells of the blood–brain barrier (Ambudkar *et al.*, 2003). This glycoprotein decreases intracellular and brain tissue concentrations, therefore it is likely to modulate beneficial effects as well as some toxic effects of γ-Sec-I, potentially compromising safety margins (*c.f.*, higher exposure in target organ systems such as the spleen, where P-glycoprotein is not expressed). It is not clear to what extent this interaction can modulate intracellular exposure in globlet or progenitor cells when high local concentrations following i.p. or oral administration could lead to saturation of transport. The extent of efflux was similar for BZ and DBZ *in vitro* (intermediate); AS was not a substrate of P-glycoprotein. Although differences in P-glycoprotein efflux do not appear to explain differences in susceptibility to gut toxicity, it would be interesting to establish whether mice that are genetically deficient in mdr1a P-glycoprotein would show greater sensitivity.

In a time-course evaluation, using the mid-dose BZ, the severity of metaplastic changes in the gut progressed temporally throughout the small and large intestines, although this effect was less severe in the large intestine. This may be due to the endogenous population of goblet cells being greater in the more distal parts of the gut, thus masking the effect of goblet cell metaplasia. Alternatively, the compounds may be peculiarly effective in causing goblet cell metaplasia of higher parts of the intestinal tract. The lack of metaplasia in the cecum was considered to be due to the presence of typhlitis from day 3. This inflammatory change was considered to be secondary to gut perturbation in the small intestine rather than a consequence of intraperitoneal injection, and this concept is consistent with the fact that no typhlitis was observed in control animals. Intestinal crypt epithelial and glandular epithelial apoptosis was observed on days 1–5, followed by metaplasia on days 2–5, and crypt epithelial and glandular epithelial regeneration on days 4–5. We did not test whether the effects of these compounds were reversible.

Using expression data for separating chemical toxicity from pharmacology is an important goal in toxicology. To do that with this work, one would compare expression profiles of AS samples to BZ samples. Expression profiling revealed significant mRNA expression changes in samples taken from animals dosed with BZ in the time-course study. We do not have AS array time-course data or DBZ 5-day data. However, we did perform

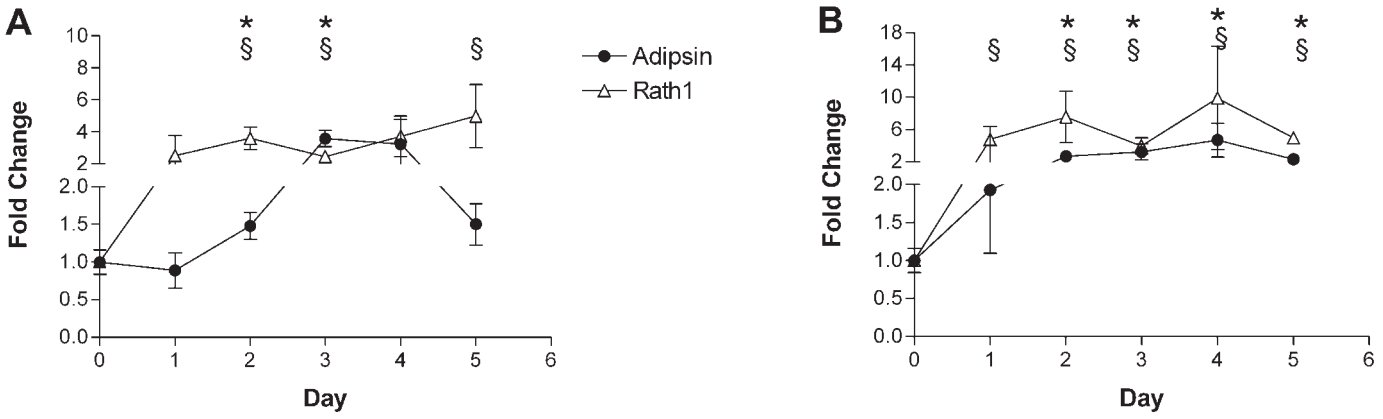

FIG. 7. Real-time polymerase chain reaction analysis of Rath1 and adipsin transcripts in duodenum total RNA from two independent 5-day time-course experiments. (A) Experiment A time-course evaluation of samples taken from animals dosed with 30 μmol/kg b.i.d. BZ for 1–5 days. $n = 3$ for all time points except day 2 ($n = 2$). (B) Experiment B time-course evaluation of samples taken from animals dosed with 30 μmol/kg b.i.d. BZ for 1–5 days. $n = 3$ for all time points. The symbols § and * indicate $p < 0.05$ for Rath1 and adipsin, respectively, in an unpaired *t*-test that compared treatments vs controls where $n = 3$.

array analysis of samples from animals dosed with 10–100 μmol/kg AS and BZ for 5 days. Despite the comparison between a single day's readout to that from a time course, quite a few of the changes observed in the time-course study with mid-dose BZ treatment were recapitulated on day 5 in the BZ dose–response study. By contrast, we saw no statistically significant changes in mRNA expression with the AS samples when compared to controls. Thus, the lesions caused by BZ and the attendant gene expression profiles described here appear to be pharmacology (mechanism-based) related only. This conclusion is based on the correlation of Notch modulatory potency with lesion severity (DBZ > BZ, no response with AS), on the remarkable qualitative similarity in these unusual lesions observed between the different chemistries, and on the fact that there are no other adverse effects to report than those described here. Because no gene expression changes, marker increases, or lesions were attributed to AS we cannot at this time relate by comparison to AS any expression changes with BZ to chemistry or to other nonspecific effects.

Expression changes with BZ treatment included several deregulated panendocrine, hormonal and transcription factors that are a consequence both of altered Notch processing and altered differentiation of duodenal gastrointestinal secretory lineages. Pathological change (altered differentiation) was marked by upregulation of mucin, somatostatin, secretin, and CCK mRNAs by BZ at higher doses on day 5. Many of these changes with BZ were previously reported by Searfoss *et al.* (2003) and are supported by the immunohistochemical observation reported here of increased intestinal neuroendocrine cells, particularly at days 3–5 after compound administration. Unfortunately, the predictive value of these day-5 data are limited. When the changes are greatest they may be relatively late; they appear to be a function of lesion development; certainly, they cannot predict outcome or serve as premonitory markers of toxicity. Many toxic mechanisms that result from multicomponent cascades play out over time, rendering as uninformative snapshot views of transcription at single or late time points. So, to identify earlier, more predictive changes, the time-course evaluation was performed and early changes were identified. Coincident with apoptosis in intestinal crypts and glands on day 1, an mRNA signature of 'early-predictive' changes was identified; it preceded the appearance of goblet cell metaplasia and remained altered throughout the 5-day treatment period (several enteroendocrine genes were in fact upregulated at least twofold as early as day 2). Among the changes noted were the marked induction of the Hes-regulated transcriptional activator of gut secretory lineage differentiation Rath1, as well as induction of Delta1 (Notch) ligand, furin, and NeuroD mRNAs in the Notch pathway.

The mechanistic significance of the Rath1, Delta1, and NeuroD findings in their relationship to regulation of intestinal differentiation and goblet metaplasia is underscored in part by the literature on gene deletion of bHLH proteins and Notch pathway constituents including Hes1 (Jensen *et al.*, 2000), neurogenin 3 (Jenny *et al.*, 2002), NeuroD (Mutoh *et al.*, 1997; Naya *et al.*, 1997), and Math1. The balance between positive regulator bHLH proteins and Hes1 will determine both exocrine and endocrine cell differentiation. Hes1 is a basic helix-loop-helix (bHLH) transcriptional repressor that is expressed in most undifferentiated cells; it is essential for their maintenance and is required for precursor pool expansion. It inhibits differentiation of many cell types by repressing the transcription of other factors, including the bHLH transcription factor Math1 (encoded by Atoh1) (Kageyama *et al.*, 2000).

In contrast to the robust data set for Rath1, we analyzed the mRNA expression of Hes1 in duodenal samples and achieved mixed results. In the 5-day exposure study, real-time PCR analysis revealed consistent decreases in Hes1 mRNA at all doses in samples from animals dosed with BZ and another potent Notch-modulating γ-Sec-I (which also caused goblet cell

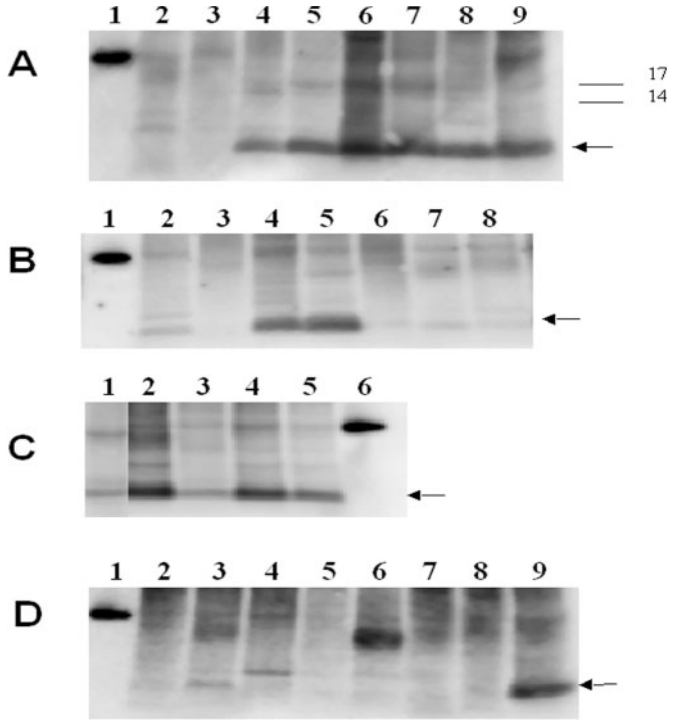

FIG. 8. Western blot detection of a rat fecal anti-adipsin reactive 6 kDa protein showing both time-dependent (1–5 days) and dose-dependent (0, 10–100 μmol/kg b.i.d. BZ, 5 days) increases caused by Notch-modulating γ-Sec-I treatment. For this study, 50 μg fecal extract proteins/lane were resolved on 4–12% NuPage Novex Bis-Tris and blotted on PVDF membranes as described in the *Methods and Materials*. Membranes were probed with Novex sheep anti-human complement factor D (adipsin) IgG using a dilution of 1:10,000. Blot A (5 day exposure study): lane 1, 20 ng human adipsin (25 kDa); lanes 2–3 vehicle control samples; lanes 4–5, extracts from individual animals dosed with 10 μmol/kg b.i.d. BZ; lanes 6–8, extract from individual animals dosed with 30 μmol/kg b.i.d. BZ; lane 9, sample from individual animal dosed with 100 μmol/kg b.i.d. DBZ. Blot B (time course: fecal extract was taken from animals dosed with 30 μmol/kg b.i.d. for 1–5 days BZ): lane 1, 20 ng human adipsin; lanes 2–3, vehicle control samples pooled from two animals each on days 3 and 1; lanes 4–5 samples pooled from two animals each on day 4; lanes 6–8, samples pooled from two animals each on days 3–1, respectively. Blot C (5-day exposure study): lane 1, pool from three vehicle control animals; lanes 2–3, samples from individual animals dosed with 10 μmol/kg b.i.d. DBZ; lanes 4–5 samples from individual animals dosed with 30 μmol/kg b.i.d. DBZ; lane 6, 20 ng human adipsin. Blot D (1-month exposure study): lane 1, 20 ng human adipsin; lane 2, pool from two vehicle control animals; lane 3, pool from two vehicle control animals; lane 4, sample from a separate individual vehicle control animal; lanes 5–8, samples taken from individual animals dosed with 100 μmol/kg b.i.d. AS; lane 9, sample taken from individual animal dosed with 100 μmol/kg b.i.d. DBZ for five days. The arrow points to the adipsin-reactive 6 kDa protein.

metaplasia but is not described here), more variably but downward with DBZ, and not with AS. Like that reported by Searfoss *et al*. (2003), we also observed in a 5-day time-course study a time-dependent and marked reduction in Hes1 mRNA with mid-dose BZ treatment (data not shown). Yet, despite a downward trend, the magnitude of changes was quite variable in a repeated independent *in vivo* time-course investigation, even as Rath1 and adipsin transcript changes in the identical RNA samples were reproduced across the two time-course trials (Fig. 7). We cannot at this time offer either a technical or a biological explanation for this discrepancy (*e.g.*, Hes1 mRNA half-life or stability sensitivity to minimal procedural changes).

In Hes1-deficient mice the expression of positive bHLH genes such as Delta1 (in an apparent positive feedback response), Neurogenin3, NeuroD, and Atoh1/Math1 are upregulated in the gut, and endocrine cells differentiate prematurely. Neurogenin 3 expression is required further downstream in the secretory lineage and is strictly required for the first steps in enteroendocrine differentiation (Jenny *et al*., 2002), and NeuroD specifies the terminal differentiation of enteroendocrine precursors to secretin and CCK-synthesizing cell types (Mutoh *et al*., 1997; Naya *et al*., 1997). Mice deficient in Hes-1 exhibit increased numbers of gastrointestinal secretory lineage goblet cells, Paneth cells, and enteroendocrine cells. The entry of stem cells into the cell cycle is generally thought to result in renewal, differentiation, or apoptosis. Thus, despite the finding that Hes-1 deficiency did not appear to affect precursor pool expansion in the gut, increased apoptosis was observed in intestinal crypts and is consistent with this principle (Jensen *et al*., 2000). In contrast to Hes1, loss of Math1 depletes secretory lineage cells (Yang *et al*., 2001).

Although rigorous proof is lacking that altered Notch signaling is the primary or sole mechanism producing the intestinal lesions described, the early Rath1, Delta1, and NeuroD upregulation described here provides a compelling case that the Rath1-dependent Notch pathway alteration is the mechanistic link to the observed gut metaplasia. This is further underscored by the report suggesting that Hes1-dependent, Math1-independent cofactors are required for specification of the endocrine lineage in uncommitted progenitors in stomach and pancreas (Yang *et al*., 2001). Rath1 is not expressed in mouse, human, or rat pancreas, or in stomach tissues, where Hes-1 deficiency is known to cause enteroendocrine architectural changes but where no lesions were detected in this study. It is possible that lesions were not detected in these tissues because the cell turnover is lower and the expression of toxicity requires more exposure time.

The identification of biomarkers of toxicity validated in animal models can mitigate risk of clinical toxicity by permitting careful dose escalation studies where therapeutic margins are expected to be narrow and early withdrawal if clinical toxicity is approached. Biomarkers can also be used in counter-screening of drug project back-ups in the discovery of novel drug series. To these ends, we confirmed that Rath1 mRNA and adipsin mRNA may serve as preclinical premonitory markers and that anti-Rath1–reactive and anti-adipsin–reactive proteins may serve as early noninvasive toxicity (reporter) biomarkers of intestinal goblet metaplasia. It is presumed that the levels of Rath1 and adipsin in feces are dependent on relative cell turnover, residence time of feces, and expression of these proteins in specific parts of the gut. Which component contributes greatest to the

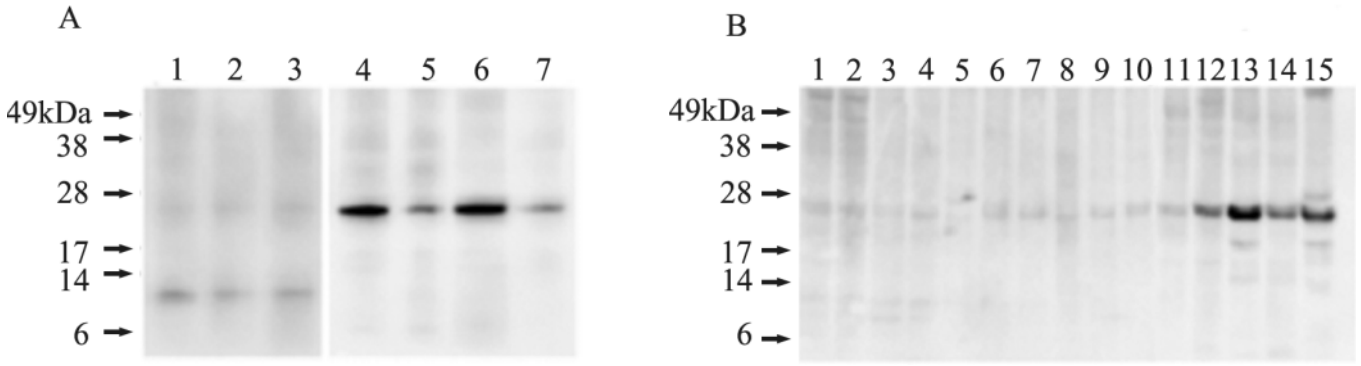

FIG. 9. BZ and DBZ caused increase abundance of anti-Rath1–reactive protein in fecal extracts of treated rats. Each lane in these experiments was loaded with 12.5 μg fecal extract protein and probed with a rabbit anti-Math1 antibody. (A) Samples taken from individual rats treated with 10 and 30 μmol/kg b.i.d. DBZ. Vehicle-treated controls are in lanes 1, 2, and 3. Lanes 4 and 5 are 10 μmol/kg b.i.d. DBZ. Lanes 6 and 7 are 30 μmol/kg b.i.d. DBZ. (B) 5-day time course of rats treated with 30 μmol/kg b.i.d. BZ. Vehicle-control samples are in lanes 1, 2, and 3; day 1 BZ, lanes 4, 5, 6, and 7; day 2 BZ, lanes 8, 9, and 10; day 3 BZ, lanes 11 and 12; day 4 BZ, lanes 13 and 14; day 5, lane 15. Pooled samples were analyzed in Day 2, lane 10; Day 3, lane 11; Day 4, lane 13; and Day 5, lane 15.

levels of these proteins in feces under metaplastic conditions is not yet known.

Rath1 and adipsin may play important roles in the pathogenesis of the metaplastic phenotype and may potentially be exploited as specific, sensitive, and noninvasive clinical biomarkers of both Notch modulation and early drug-induced goblet cell intestinal metaplasia. The predilection for drug-induced goblet cell metaplasia to affect primarily the gastrointestinal tract, a tissue with high cell turnover, suggests that early upregulation of these proteins may be detectable in the feces of patients with early metaplastic changes. Validation of these potential biomarkers in animal models and man is therefore also warranted.

SUPPLEMENTARY DATA

The short gene list shown in Table 4 is also available as MAS 5.0 raw Affymetrix signal for individual duodenal samples taken from the BZ time-course animals and from 5-day endpoint vehicle control, 10, 30, and 100 μmol/kg b.i.d. AS and BS dosed animals.

ACKNOWLEDGMENTS

We acknowledge the excellent technical contributions of James Hulsizer, Gary Moore, and Keith Herzog in synthesizing the compounds used in this study; of Mark Eisman in performing the bioanalytical analysis of drug in plasma; of Qiaoling Jiang in running the SuPT1 Notch assays; of Anne Thomas and Richard Jenkins in performing special stains and immunohistochemistry; and of Amanda Ellis in conducting the MDR1-MDCK assay.

REFERENCES

Ambudkar, K. V., Kimchi-Sarfaty, C., Sauna, Z. E., Gottessman, M. M. (2003). P-glycoprotein: from genomics to mechanism. *Oncogene* **22,** 7468–7485.

Baron, M. (2003). An overview of Notch signalling pathway. *Cell Dev. Biol.* **14,** 113–119.

Dovey, H. F., John, V., Anderson, J. P., Chen, L. Z., de Saint Andrieu, P., Fang, Freedman, L. Y., Folmer, S. B., Goldbach, B., Holsztynska, E., *et al*. (2001) Functional gamma-secretase inhibitors reduce β-amyloid peptide levels in brain. *J. Neurochem.* **76,** 173–181

Holcomb, L. A., Gordon, M. N., Jantzen, P., Hsiao, K., Duff, K., and Morgon, D. (1999) Behavioral changes in transgenic mice expressing both amyloid precursor protein and presenilin-1 mutations: Lack of association with amyloid deposits. *Behav. Genet.* **29,** 177–185.

Jenny, M., Uhl, C., Roche, C., Duluc, I., Guillermin, V., Guillemot, F., Jensen, J., Kedinger, M. and Gradwohl, G. (2002). Neurogenin3 is differentially required for endocrine cell fate specification in the intestinal and gastric epithelium. *EMBO J.* **21,** 6338–6347.

Jensen, J., Pedersen, E. E., Galante, P., Hald, J., Heller, R. S., Ishibashi, M., Kageyama, R., Guillemot, F., Serup, P., and Madsen, O. D. (2000). Control of endodermal endocrine development. *Nat. Genet.* **24,** 36–44.

Jung, K-M., Tan, S., Landman, N., Petrova, K., Murray, S., Lewis, R., Kim, P. K., Kim, D. S., Ryu, S. H., Chao, M. V., and Kim, T-W. (2003). Regulated intramembrane proteolysis of the p75 neurotrophin receptor modulates its association with the TrkA receptor. *J. Biol. Chem.* **278,** 42161–42169.

Kageyama, R., Ohtsuka, T., and Tomita, K. (2000). The bHLH Gene Hes1 regulates differentiation of multiple cell types. *Mol. Cell* **10,** 1–7.

LaVoie, M. J., and Selkoe, D. J. (2003). The Notch ligands, Jagged and Delta, are sequentially processed by γ-secretase and presenilin/γ-secretase and release signalling fragments. *J. Biol. Chem.* **278,** 34427–34437.

Lee C., Perreault N., Brestelli J., and Kaestner, K. (2002). Neurogenin 3 is essential for the proper specification of gastric enteroendocrine cells and the maintenance of gastric epithelial cell identity. *Genes Dev.* **16,** 1488–1497.

Marambaud, P., Wen, P. H., Dutt, A., Shioi, A. T., Siman, R., and Robakis, N. K. (2003). A CBP binding transcriptional repressor produced by the PS1/ε—cleavage of N-cadherin is inhibited by PS1 FAD mutations. *Cell* **114,** 635–645.

Mutoh, H., Fung, B. P., Naya, F. J., Tsai, M-J., Nishitani, J., and Leiter, A. B. (1997). The basic helix–loop–helix transcription factor BETA2yNeuroD is expressed in mammalian enteroendocrine cells and activates secretin gene expression. *Proc. Natl. Acad. Sci. U.S.A.* **94,** 3560–3564.

Naya, F. J., Huang, H. P., Qiu, Y., Mutoh, H., DeMayo, F. J., Leiter, A. B., and Tsai, M. J. (1997). Diabetes, defective pancreatic morphogenesis, and

abnormal enteroendocrine differentia tion in BETA2/neuroD-deficient mice. *Genes Dev.* **11,** 2323–2334.

Okamoto, I., Kawano, Y., Murakami, D., Sasayama, T., Araki, N., Miki, T., Wong, A. J., and Saya, H. (2001). Proteolutic release of CD44 in the intracellular domain and its role in the CD44 signalling pathway. *J. Cell. Biol.* **155,** 755–762.

Polli, J. W., Wring, S. A., Humphreys, J. E., Huang, L., Morgan, J. B., Webster, L., and Serabjit-Singh, C. S. (2001). Rational use of *in vitro* P-glycoprotein assays in drug discovery. *J. Pharmacol. Exp. Ther.* **299,** 620–628.

Ray, W., Yao, M., Mumm, J., Schroeter, E. H., Saftig, P., Wolfe, M., Selkoe, D. J., Kopan, R., and Goate, A. M. (1999). Cell surface presenilin-1 participates in the γ-secretase-like proteolysis of Notch. *J. Biol. Chem.* **274,** 36801–36807.

Sasai, Y., Kageyama, R., Tagawa, Y., Shigemoto, R., and Nakanishi, S. (1992). Two mammalian helix–loop–helix factors structurally related to Drosophila hairy and Enhancer of split. *Genes Dev.* **6,** 2620–2634.

Searfoss, G. H., Jordan, W. H., Calligaro, D. O., Galbreath, E. J., Schirtzinger, L. M., Berridge, B. R., Gao, H., Higgins, M. A., May, P. C., and Ryan, T. P. (2003). Adipsin: A biomarker of gastrointestinal toxicity mediated by a functional γ-secretase inhibitor. *J. Biol. Chem.* **278,** 46107–46116.

Selkoe, D. J. (2001) Alzheimer's disease: Genes, proteins, and therapy. *Physiol. Rev.* **81,** 741–766.

Wong, G. T., Manfra, D., Poulet, F. M., Zhang, Q., Josien, H., Bara, T., Engstrom, L., Pinzon-Ortiz, M., Fine, J. S., Le, H-J. J., Zhang, L., Higgins, G. A., and Parker, E. M. (2004). chronic treatment with the γ-secretase inhibitor LY-411,575 inhibits β-amyloid peptide production and alters lymphopoiesis and intestinal cell differentiation. *J. Biol. Chem.* **279,** 12876–12882.

Yang, Q., Bermingham, N. A., Finegold, M. J., and Zoghbi, H. Y. (2001). Requirement for Math1 for secretory cell lineage commitment in the mouse intestine. *Science* **294,** 2155–2158.